Graph learning for functional brain connectivity: An empathy network study

A thesis submitted in partial fulfillment
of the requirements for the degree of

Master of Science
in
Electronics and Communication Engineering by Research

by

Sasanka GRS
2019112017
sasanka.grs@research.iiit.ac.in

Advisor: Dr. Santosh Nannuru

INTERNATIONAL INSTITUTE OF
INFORMATION TECHNOLOGY
HYDERABAD

International Institute of Information Technology Hyderabad
500 032, India

June 2024

International Institute of Information Technology Hyderabad
Hyderabad, India

CERTIFICATE

This is to certify that work presented in this thesis proposal titled ***Graph learning for functional brain connectivity: An empathy network study*** by *Sasanka GRS* has been carried out under my supervision and is not submitted elsewhere for a degree.

Date

Advisor: Dr. Santosh Nannuru

To my family and friends

Acknowledgement

I would like to express my sincere gratitude to my research advisor, Dr. Santosh Nannuru, for his constant support, invaluable guidance, and mentorship throughout my research journey. His expertise, encouragement, and dedication have been helpful in shaping my academic and professional growth, providing me with the necessary skill-set and knowledge for future endeavours. I am truly fortunate to have had the opportunity to work under his guidance.

I am also immensely grateful to my collaborators, Ayushi Agrawal and Dr. Kavita Vemuri, for their invaluable contributions, support, and collaboration throughout the research process.

I would like to express my heartfelt appreciation to my family, particularly my parents, for their love, encouragement, and support throughout my academic journey. I want to express my gratitude to my father for sparking my interest in research and always inspiring me, and my mother, for the emotional support throughout. I would like to express my love and gratitude to my brothers, Chandraaditya, Saketh and Kaarthikeya for being my companions throughout the journey.

I would also like to extend my heartfelt thanks to my close friends, Samruddhi, Viswanadh, Niteesh, Usha, Ayu, Spanddhana, Sasanka Uppuluri and Sresthavadhani, for their support and encouragement. Their friendship and support have been a constant source of strength and joy throughout my research journey, and I treasure the memories made.

Additionally, I would like to acknowledge my lab mates, Shreyash, Om, Nagesh, Ritik, Shreyas Jaiswal and Chetan. Their enthusiasm, dedication, and positive energy have created a healthy and fun atmosphere in the lab. I am grateful for their friendship, support, and the sense of community we share, which has made my research journey both rewarding and enjoyable. I extend my wishes to the new researchers - Ashwini, Chandana, Aadarsh and Aditya.

Lastly, I sincerely appreciate everyone who has supported, encouraged, and believed in me throughout this journey.

Abstract

Functional Magnetic Resonance Imaging (fMRI) research employing naturalistic stimuli, particularly movies, examines brain network interactions underlying complex cognitive processes such as empathy. Leveraging graph learning methods applied to whole-brain time-series signals, a novel processing pipeline is proposed, integrating high-pass filtering, voxel-level clustering, and windowed graph learning with a sparsity-based approach. The study involves the analysis of fMRI data collected from healthy participants while watching empathetic movies and during resting-state conditions. Key brain regions implicated in the empathy network, including the Insula, Pre-Frontal Cortex (PFC), Anterior Cingulate Cortex (ACC), and parietal regions, are examined.

Results of the exploratory analysis reveal that the sparsity-based graph learning method consistently outperforms others in capturing graph cluster label variations in comparison with the emotion contagion scale, achieving over 88% match across participants. The analysis demonstrates a gradual induction of empathy with a match after 150 seconds through the stimulus. Additionally, edge-weight dynamics analysis of the edge between empathy supporting areas underscores the superiority of sparsity-based learning, with some providing noisy activations. Connectome-network analysis highlights the pivotal role of the Insula, Amygdala, and Thalamus in empathy, with lateral brain connections facilitating synchronized responses. Spectral filtering analysis emphasizes the significance of the band-pass filter in isolating regions linked to emotional and empathetic processing during high emotional states. Strong similarities across movies in graph cluster labels, connectome-network analysis, and spectral filtering-based analyses reveal robust neural correlates of empathy.

Furthermore, a comparative study of task and resting-state conditions reveals alignment with the resting-state during low emotional valence intervals of the movie but diverges notably during high emotional valence intervals, suggesting a shared connectivity pattern between stimulus-induced directed (controlled) mind wandering *(bottom-up process)* and resting-state activity *(top-down process)*. The sparsity-based method shows a 98% match with viewer ratings on the emotion contagion scale, surpassing the 84% match achieved by Pearson's correlation-based method. This nuanced understanding of neural dynamics in empathy-related tasks versus resting-state enhances the understanding of the networks underlying cognitive processes in real-life situations (naturalistic) and the use of resting-state for the same, paving way for targeted interventions and treatments for conditions associated with empathetic processing and offering significant real-life applications and impact.

Contents

List of Figures

List of Tables

Abbreviations

3D	3 Dimensional
4D	4 Dimensional
AAL	Automated Anatomical Labelling
ACC	Anterior Cingulate Cortex
Avg	Average
BOLD	Blood Oxygen Level Dependent
BPF	Band Pass Filter
DMN	Default Mode Network
EEG	Electroencephalogram
FCD	Functional Connectivity Density
FIR	Finite Impulse Response
fMRI	Functional Magnetic Resonance Imaging
GCN	Graph Convolutional Network
GFT	Graph Fourier Transform
GLM	General Linear Model
GNN	Graph Neural Network
GSP	Graph Signal Processing
HPF	High Pass Filter
ICA	Independent Component Analysis
IGFT	Inverse Graph Fourier Transform
IIIT	International Institute of Information Technology
IRB	Institutional Review Board
ISC	Inter-Subject Correlation
LPF	Low Pass Filter
M1	Movie 1
M2	Movie 2
MVPA	Multi-Voxel Pattern Analysis
PCC	Anterior Cingulate Cortex
PFC	Pre-Frontal Cortex

Rs	Rupees
SPM	Statistical Parametric Mapping
TFA	Time-Frequency Analysis
TR	Repetition Time

Symbols

$\mathcal{G}$	Graph
N	Number of nodes
$\mathcal{N}$	Set of nodes
$\mathcal{E}$	Set of edges
$\mathbf{N}$	Graph adjacency matrix
$\mathbf{L}$	Graph Laplacian matrix
$\mathbf{D}$	Graph Degree matrix
$\mathbf{x}$	Graph signal
$\mathbb{R}^N$	Set of real vectors of dimension N
$\mathbf{x}[n]$	Signal at node n
P	Length of signal at each node
$\mathbf{X}$	Graph signal matrix / data
$\mathbf{X}[n]$	P dimensional signal at node n
$\mathbf{X}_p[n]$	p-th signal at node n
$\mathbf{U}$	Eigenvector matrix of graph Laplacian
$\mathbf{\Lambda}$	Eigenvalue matrix of graph Laplacian
λ_l	l-th eigenvalue of graph Laplacian
$\mathbf{u}_l$	l-th eigenvector of graph Laplacian
$\hat{\mathbf{x}}$	Graph Fourier Transform coefficients
$\hat{\mathbf{x}}[l]]$	l-th Graph Fourier Transform coefficient
λ_c	Cut-off graph frequency for low-pass and high-pass filters
λ_1	Lower cut-off graph frequency for band-pass filter
λ_2	Upper cut-off graph frequency for band-pass filter
$\approx$	Approximately
$Fstop$	Stop-band cutoff of FIR filter
$Fpass$	Pass-band cutoff of FIR filter
$Wstop$	Stop-band weight of FIR filter
$Wpass$	Pass-band weight of FIR filter
$dens$	Density factor of FIR filter

K	Number of clusters for clustering
ρ	Pearson's correlation coefficient
$\mu_{\mathbf{X}[n]}$	Mean of signal $\mathbf{X}[n]$
$\sigma_{\mathbf{X}[n]}$	Standard Deviation of signal $\mathbf{X}[n]$
d_{nm}	Distance between nodes n and m
σ	Hyperparameter for distance-based graph learning
ℓ_1	L1 norm
ℓ_2	L2 norm
$\mathbf{Y}$	Data fit over learnt graph in smoothness-based graph learning
α	Hyperparameter for smoothness term in smoothness-based graph learning
β	Hyperparameter for data fidelity term in smoothness-based graph learning
$\boldsymbol{\beta_n}$	Adjacency vector of node n to all other nodes in sparsity-based graph learning
λ	Hyperparameter for sparsity term in sparsity-based graph learning
$\mathbf{B}$	Non-symmetric graph adjacency matrix in sparsity-based graph learning
$\leftrightarrow$	Connected edge between two regions
\$	US Dollars

List of Related Publications

[P1] S. GRS, A. Agrawal, S. Nannuru and K. Vemuri **"Graph learning methods to extract empathy supporting regions in a naturalistic stimuli fMRI"**, submitted to *Brain and Cognition*, 2024.

[P2] S. GRS, A. Agrawal, S. Nannuru and K. Vemuri **"Comparing task-based and resting-state brain networks: A graph learning approach for naturalistic stimuli fMRI"**, submitted to *Brain Connectivity*, 2024.

Chapter 1

Introduction

1.1 Motivation

Empathy is our ability to take the perspective and share the emotions and feelings of others. Empathizing includes mentalizing or cognitive evaluation and emotional response, making it a complex construct to study from behaviour and brain activity. Learning empathy is essential as it is integral to many aspects of human behavior, such as interpersonal interactions and moral development. Prosocial behaviors like care and interaction are facilitated by empathy and are necessary for maintaining constructive relationships.

A number of psychopathological disorders, such as conduct disorders, schizophrenia, and autism spectrum disorders, have been associated with empathy deficits [1,2]. Thus, understanding human social behavior, emotional processing, and mental health requires an understanding of empathy. Investigations over the cognitive processes underlying empathy would contribute to a comprehensive understanding of the neural processing concerning empathetic responses, paving way for targeted interventions and treatments for conditions associated with empathetic processing.

From a regional activation perspective, empathy involves multiple regions contributing to a multi-faceted response to an emotional stimulus, deprecating the use of traditional regional activation analyses. Graph Signal Processing (GSP) allows a nuanced exploration of connections between different regions, capturing the brain's dynamic network. Modelling the brain as a graph unveils patterns governing coordinated activity, fitting the brain's interconnected nature during a multi-modal stimulus.

GSP [3] is a versatile field that merges graph theory, linear algebra, and signal processing to analyze signals on graphs, offering a robust framework for extracting insights from networked data. The tools offered by GSP present the data in an irregular graph domain unlike the conventional time and frequency domains, opening a spectrum of applications over the data represented across graph nodes. GSP finds its applications in scenarios where the data can be overlaid onto a set of nodes and the edges model interactions between them.

The edges of the graph can either be existing, making the graph an apriori knowledge or they can be learnt from the data over the nodes referred to as the graph signals. The process of constructing the graph from the data is termed as graph learning. The process of making connections between nodes depends on the application of a similarity metric, wherein the strength of an edge is quantified by the strength of similarity between signals at the respective nodes. Some well-known methods of graph learning, of interest for this work are detailed in Chapter 5 Section 4.5.

Utilizing GSP and graph learning is motivated by the brain's intricate functional organization. Unlike traditional approaches that focus solely on specific brain regions, GSP enables a detailed examination of the connections between various brain areas, thus capturing the dynamic network of the brain. Graph Fourier Transform (GFT) goes beyond traditional GSP by incorporating both signal properties and graph properties. It allows us to understand not only how signals change across the nodes of a graph but also how different frequency components contribute to these changes. GFT's spectral bands serve distinct purposes: the low-pass band emphasizes brain regions associated with global network dynamics and slower oscillatory patterns, such as Default Mode Network (DMN) regions, the high-pass band explores deeper localization, while the band-pass band strikes a balance, identifying patches without extremes, making it interesting for empathy-related brain activity exploration. Applying GFT aligns with our objective to understand empathy-specific regions efficiently.

Further, in fMRI research, the investigation of connectivity patterns during tasks as compared to resting-state is critical for understanding the differences in neural activation. We can understand the brain by *localization*, that is looking at functions of certain regions of interest or by *connectivity*, where the interest is to understand connections between spatially segregated areas. Both the analysis provide valuable insights for a task paradigm with stimuli, the *connectivity* is explored for resting-state data. Resting-state captures brain function when subjects are not focused on a task and reveals brain networks involved in *top-down* processing. *Top-down* processing refers to the directional flow of information within the brain, from higher-level brain regions to lower-level regions. Regions of the brain responsible for functions such as attention, memory, and decision-making are known to influence lower-level sensory regions, altering their activity even in the absence of external input [4]. In contrast, task-fMRI engages focused brain functions like memory, emotions, language, decision-making, and sensory-differentiation, making it both *bottom-up* and *top-down* processing. *Bottom-up* processing refers to the directional flow of information from sensory regions at lower neural levels towards cognitive regions situated at higher neural levels. This includes the initial encoding and evaluation of sensory stimuli, subsequently guiding the activation of advanced cognitive functions and behavioral responses [4].

1.2 Summary of contributions

This work contributes a signal processing pipeline to extract functional connectivity networks from raw fMRI BOLD data and analyse them according to the task in hand. The details and two applications of the pipeline are detailed in this work in three chapters.

- Chapter 4 introduces the proposed signal processing pipeline to extract dynamic functional connectivity networks from raw fMRI BOLD data. The fMRI signal processing pipeline presented in this work processes raw fMRI BOLD signals by modularizing data extraction from voxel-level to region-level, subsequently extracting functional connectivity networks in a windowed manner. Optimization problems are employed to derive functional connectivity matrices from data over time-windows, while denoising is achieved through high-pass filtering and phase-based voxel clustering.

- Chapter 5 presents an application of the proposed pipeline in analysing empathy in the brain. This work investigates brain network states and empathy-related brain activity in response to naturalistic stimuli, highlighting sparsity-based graph learning approach. It contrasts traditional regional activation studies, revealing alignment with the emotion scale (detailed in Chapter 5) and highlighting key brain regions associated with empathy like Insula, ACC and Amygdala. Comparisons of empathy-related brain activity between two movies identify common regions with a stronger foundation in eliciting empathetic responses.

- Chapter 6 presents another application of the proposed pipeline in comparing task-based and resting-state networks in the brain. This study demonstrates the correlation between time-varying graph-dissimilarity metrics and the emotion scale (detailed in Chapter 5), highlighting similarities and dissimilarities between task-based and resting-state networks across different emotional intervals. Further validation is provided through connectome-network analysis, revealing overlapping highlighted edges during low-emotion intervals in both networks. Overall, the findings confirm the hypothesis on similarity between the resting-state and task-based network during low emotional intervals in the stimulus, underscoring the superior performance of the sparsity-based method in supporting this hypothesis.

These contributions provide valuable insights into neural interactions during complex tasks such as empathy, as well as a comparison with the resting-state, which holds particular significance for researchers in the field of empathy and brain research.

1.3 Organisation of the thesis

The thesis is organised into seven chapters.

- **Chapter 1 - Introduction**: Provides an overview of the research problem, motivation, and contributions of the study.

- **Chapter 2 - Related Work**: Reviews existing literature on graph learning, empathy research, resting-state study and analyse their relevance to this work.
- **Chapter 3 - Preliminaries**: Introduces fundamental concepts and background information relevant to graph signal processing, brain connectivity, and empathy.
- **Chapter 4 - fMRI processing pipeline**: Describes the proposed methodology and pipeline for analyzing raw BOLD fMRI data using graph learning techniques.
- **Chapter 5 - Graph Learning for Empathy**: Investigates the application of graph learning specifically for understanding empathy, including data collection, pre-processing, and analysis methods.
- **Chapter 6 - Graph Learning to Compare Resting State with Empathy**: Explores how graph learning can be used to compare brain connectivity patterns during resting state and empathy-inducing stimuli like movies.
- **Chapter 7 - Conclusion**: Summarizes the findings of the study, discusses implications, limitations, and future directions for research.

Note

The author was involved in developing the code base, formulating the processing pipeline, analysing the results, and formatting the manuscript for both [P1] and [P2]. Collaborators Ayushi Agrawal and Kavita Vemuri from the Cognitive Sciences Lab at International Institute of Information Technology (IIIT) Hyderabad were responsible for data collection, analysis, and interpreting the results in both [P1] and [P2]. Santosh Nannuru contributed to all the submissions by providing input on conceptualization, reviewing technical aspects, and assisting with manuscript editing and submissions.

Chapter 2

Preliminaries

2.1 Graph Signal Processing

GSP [3] is a versatile field that merges graph theory, linear algebra, and signal processing to analyze signals on graphs, offering a robust framework for extracting insights from networked data.

2.1.1 Notations

A graph $\mathcal{G}$ consists of a set of N nodes $\mathcal{N} = \{1, 2, \ldots, N\}$ and a set of edges $\mathcal{E}$. The graph connectivity is described using the adjacency matrix $\mathbf{A}$ where the (i, j)-th entry denotes the weight associated with the edge connecting nodes i and j. The graph Laplacian matrix $\mathbf{L}$ is given by $\mathbf{L} = \mathbf{D} - \mathbf{A}$ where $\mathbf{D}$ is the degree matrix, obtained by summing over rows or columns of the adjacency matrix $\mathbf{A}$. A graph signal $\mathbf{x} \in \mathbb{R}^N$ is a vector with the entry $\mathbf{x}[n]$ denoting the signal at node n of the graph. For a P dimensional signal at each node, the graph signal is an $N \times P$ matrix $\mathbf{X} = [\mathbf{x}_1, \mathbf{x}_2 \ldots \mathbf{x}_P]^T$. $\mathbf{X}[n]$ denotes all the P observations of the graph signal at node n and $\mathbf{X}_p[n]$ denotes the pth observation of the signal at node n.

An important property of the graph Laplacian arises through its eigendecomposition. Mathematically, the eigendecomposition of the graph Laplacian is given as $\mathbf{L} = \mathbf{U}\mathbf{\Lambda}\mathbf{U}^T$ where, $\mathbf{\Lambda}$ is the set of eigenvalues, while $\mathbf{U}$ is the set of eigenvectors for the corresponding eigenvalues. The eigenvalue matrix $\mathbf{\Lambda}$ is diagonal matrix with the diagonal entries consisting of the eigenvalues $\lambda_l,\ l = 0, 1, \ldots, N-1$ in the increasing order $0 \leq \lambda_1 \leq \ldots \lambda_{N-1}$, and $\lambda_0 = 0$.

2.1.2 Graph Fourier Transform (GFT) and spectral filtering

On eigendecomposition of the graph Laplacian matrix, the obtained eigenvectors show different levels of variations when overlaid on the graph. Here, we define total variation of a graph signal $\mathbf{x}$ on a graph $\mathcal{G}$ with graph Laplacian $\mathbf{L}$ as $\mathrm{TV}_{\mathcal{G}}(\mathbf{x}) = \mathbf{x}^T\mathbf{L}\mathbf{x}$, which quantifies the overall variation of the graph signal over all the edges. The eigenvectors corresponding to lower eigenvalues represent lower total variation, and vice-versa giving rise to the concept of frequencies. Considering the total variation of the eigenvectors, the corresponding eigenvalues can be interpreted as graph frequencies, or Fourier modes [3], which holds frequency information of the graph. Similarly, the set of eigenvectors $\mathbf{U}$ consists of $\mathbf{u}_l,\ l = 0, 1, \ldots, N-1$, which are the Fourier bases corresponding to the Fourier modes.

GFT of a graph signal $\mathbf{x}$ is mathematically defined as $\hat{\mathbf{x}} = \mathbf{U}^T\mathbf{x}$. The GFT transforms the signal from the graph domain to the spectral domain, capturing the frequency content of signals, revealing essential information about the underlying structure and connectivity of the graph. By decomposing a signal into its graph Fourier components, one can identify patterns, clusters, or anomalies within complex networks. Similar to the classical Fourier transform, the graph Fourier coefficient $\hat{\mathbf{x}}[l]$ serves as an indicator of the energy of the signal $\mathbf{x}$ at the corresponding graph frequency λ_l.

Just as in the classical Fourier domain, it is possible to design spectral domain filters that operate on specific graph frequencies. An ideal filter $f(\lambda)$ in spectral domain can be written as

$$f(\lambda; \lambda_{low}, \lambda_{high}) = \begin{cases} 1 & \text{if } \lambda_{low} \leq \lambda \leq \lambda_{high} \\ 0 & \text{otherwise} \end{cases} \tag{2.1}$$

where, the parameters λ_{low} and λ_{high} determine the characteristics of the filter (cutoff frequencies). The filter shown in (2.1) denotes a spectral band-pass filter with cutoffs λ_{low} and λ_{high}. Tuning $\lambda_{low} = 0$ and $\lambda_{high} = \lambda_c$ designs a spectral low-pass filter with cutoff λ_c. Tuning $\lambda_{low} = \lambda_c$ and $\lambda_{high} = \lambda_{N-1}$ designs a spectral high-pass filter. For practical use, the filter in (2.1) defined on continuous graph frequency λ is uniformly sampled to produce N samples, making it a discrete spectral filter $f_D(\lambda_l)$, operating on the graph frequencies $\lambda_l,\ l = 0, 1, \ldots, N-1$. This discrete spectral filter can be represented as an $N \times 1$ vector.

The inverse operation from the spectral domain back to the graph domain is mathematically defined as $\mathbf{x} = \mathbf{U}\hat{\mathbf{x}}$, termed as Inverse Graph Fourier Transform (IGFT). From the above definitions, a graph spectral filtering operator can be defined as

$$\mathcal{H}_{\mathbf{f_D}}\mathbf{x} = \mathbf{U}\mathbf{f_D} \odot (\mathbf{U}^T\mathbf{x}) \tag{2.2}$$

where $\mathbf{f_D}$ is the discrete spectral filter, $\odot$ represents an element-wise product.

This work explores the brain regions identified in each of these spectral bands, by splitting the graph spectrum into 3 equal-sized bands, i.e., the cutoffs $\lambda_c = \lambda_{\frac{N-1}{3}}$ for the low-pass band, $\lambda_{low} = \lambda_{\frac{N-1}{3}}$ and $\lambda_{high} = \lambda_{\frac{2(N-1)}{3}}$ for the band-pass band and $\lambda_c = \lambda_{\frac{2(N-1)}{3}}$ for the high-pass band.

The different graph spectral bands offer valuable insights into the underlying structure and dynamics of regional activations. Intuitively, the low-pass band targets stationary nodes and predominantly captures components of the signal that exhibit consistency across the entire graph, emphasizing brain regions associated with global network dynamics and slower oscillatory patterns, such as DMN regions. Conversely, the high-pass band delves into deeper localization of nodes, emphasizing dynamic changes and localized variations within the network.

Of particular interest is the band-pass band, which focuses on identifying patches within the graph. Unlike the extremes of the low-pass and high-pass bands, the band-pass band strikes a balance, highlighting regions with significant variations while avoiding the extremes. This characteristic renders it particularly useful for further analysis in this work, as it offers a nuanced perspective on the connectivity patterns associated with empathy-related brain activity.

2.2 Functional connectivity

Functional connectivity refers to the temporal alignment of neurophysiological events occurring in different regions of the brain. This concept relies on statistical associations between activity measures recorded across different brain areas, suggesting functional connectivity when there is a considerable statistical relationship between their activities, irrespective of their physical proximity. It is essential to note that functional connectivity, being purely correlative, reflects observational patterns of how activities in various brain regions coincide over time, without implying a causal connection or direct anatomical linkage between these regions.

Two regions of the brain are expected to show functional connectivity if their activation levels and patterns over a short time-interval are related above-chance. It solely relies on correlation between the activations between the regions, which can be explained through indirect anatomical pathways for signal overlay. It is crucial to distinguish functional connectivity from structural connectivity in the brain, which refers to the physical interconnection of different brain regions through white matter tracts, establishing the anatomical organization. The structural network comprises specific physical pathways linking various brain regions and provides insights into the brain's physical architecture and information transmission pathways. Though not necessary, in many cases, both structural and functional connectivity show similarities [5, 6].

Obtaining functional connectivity over a pattern-match over multiple snapshots of data is preferred, as the stochastic properties and temporal coincidences of signals cannot be captured with a single snapshot. The applications of structural connectivity are limited to providing insights about the organization of the brain (which may be useful to identify malformations in the brain [7]), while functional connectivity is capable of identifying task-based connectivity patterns, which is of interest in this work.

Among the array of methods available for assessing functional connectivity, Pearson's correlation coefficient stands out as a widely utilized approach, which we use for comparison with the proposed processing pipeline.

2.3 Graph Learning

In graph learning, the task involves obtaining the edges of a graph based on the signals generated by interactions among its constituent nodes. This process involves making informed assumptions about the nature of interactions between nodes, for example, signal smoothness, sparsity, and stationarity. These underlying assumptions serve as guiding principles that shape the resulting graph structures, with each assumption potentially generating varied graphs. Therefore, the selection of the appropriate assumption is important, necessitating a comprehensive understanding of the intrinsic properties of the signals under examination. The connections between nodes are made over a similarity metric, which governs the weight of the edge between the pair of nodes. Some well-known methods of graph learning, of interest for this work are listed below.

1. **Node-distance**-based graph learning [8] method computes the euclidean distance between the signals associated with every pair of nodes and inverts them to form the adjacency matrix of the learnt graph.

2. **Pearson-coefficient**-based graph learning [9] method models the node signals as random vectors and finds the Pearson-correlation-coefficient between signals at every node pair. The pair-wise coefficient matrix forms the adjacency matrix of the learnt graph.

3. **Sparsity**-based graph learning [8] tries to explain the signal at a given node using a sparse linear combination of signals at all the other nodes. Specifically, it solves an optimization problem for each node to extract its sparse connections which is converted into the adjacency matrix.

4. **Smoothness**-based graph construction method learns a graph such that the given graph signals tend to be smooth on the learnt graph. It solves an optimization problem to fit a learnt data, which is close to the original data, which is smooth over the learnt graph.

Detailed explanation of each of the graph learning methods are discussed in Chapter 5 Section 4.5.

Chapter 3

Related work

A wide-spectrum of prior work exists on the field of brain and cognition. This work sets itself apart from them by focusing on GSP and graph learning applications to complex constructs like empathy. The related work can be broadly categorized into four fields - naturalistic stimuli and empathy response, conventional whole-brain studies, resting state based studies and more recent studies using GSP.

3.1 Naturalistic stimuli and empathy response

Movies, whether short clips or full-length features, serve as stimuli in fMRI studies to provide a rich context and complex sensory input, enabling the examination of the temporal dynamics of brain regions. This approach allows viewers to evoke scene-dependent empathy responses, facilitating the analysis of brain activity patterns over time [10–12]. However, analyzing long-duration stimuli, such as movies, poses challenges when using traditional methods like the General Linear Model (GLM), which is typically employed to separate signal from noise and account for time-delays introduced during experimental design [10].

Task-based fMRI studies engage specific brain functions such as memory, emotion, language, decision-making, and sensory differentiation, involving both *bottom-up* and *top-down* processing. Naturalistic stimuli like movies or text narratives provide ecologically valid contexts in fMRI or Electroencephalogram (EEG) experiments, as they simulate real-life experiences, which are inherently complex. Additionally, such stimuli offer insights into brain networks involved in processing complex sensory information [13].

Empathy, defined as the ability to understand and share others' emotions or feelings, entails both *top-down* processing, such as mentalizing or cognitive evaluation of others' mental states, and *bottom-up* processing, including emotional responses and self-evaluation contexts [13]. Research on empathy has explored various conditions such as Autism spectrum disorder [14], psychopathy [15], age-related differences [16], and social interactions [17]. Recent studies have emphasized the role of context or situational settings in influencing differential empathy responses [13].

Using techniques like fMRI, studies have identified several brain regions consistently implicated in empathy-related processes. These regions include the ACC, associated with decision-making, social cognition, judgments, and emotion regulation; the Insula, crucial for emotion processing, self-awareness, introspection, and pain empathy; the Inferior frontal gyrus, supporting functions like language processing, memory, and cognitive judgments of others' emotional states; the Amygdala, particularly involved in fear processing; and the Superior temporal gyrus and Somatosensory cortex, along with regions forming the DMN, which contribute to empathy networks in the brain [18–22].

3.2 Conventional whole-brain studies

To investigate whole-brain dynamics in response to naturalistic stimuli, researchers have employed various statistical methods, each with its own advantages and limitations. Independent Component Analysis (ICA) is frequently used, leveraging blind source separation to decompose the fMRI signal into spatially independent components and their associated time courses [23]. While ICA offers the advantage of capturing temporally correlated component maps, its consistency can be affected by non-deterministic algorithms, posing a challenge to reproducibility. Another approach is Functional Connectivity Density (FCD) analysis, which quantifies the correlation between voxel signals without relying on specific pathways. However, FCD analysis often requires additional multivariate pattern analysis and can be computationally intensive.

Further, Multi-Voxel Pattern Analysis (MVPA) and Inter-Subject Correlation (ISC) have been widely utilized in task-based fMRI studies [24,25]. MVPA examines patterns of activity across multiple voxels to decode cognitive states or stimuli representations, offering insights into the distributed neural representations underlying cognitive processes. On the other hand, ISC assesses the consistency of brain activity across participants, revealing shared neural responses to stimuli or tasks. While MVPA and ISC provide valuable insights into brain function and inter-subject variability, they also have limitations, such as the need for large datasets to achieve robust results and challenges in interpreting complex patterns of activity.

Neural networks [26–29] have also been employed due to their ability to approximate complex functions and adapt to nonlinear problems. However, these models require careful architecture design and parameter tuning, and their performance heavily depends on the availability of large datasets for training. Task-based fMRI studies, which typically involve a limited number of participants, may not provide sufficient data for effective training and generalization. In recent years, deep learning [30–32] approaches have gained popularity for analyzing fMRI data due to their strong expressive ability and suitability for processing complex information. However, deep learning models also demand large datasets for training and substantial computing resources, posing challenges for task-fMRI studies with limited participant numbers. Moreover, the interpretability of deep learning models can be limited, and their training and tuning processes are often complex and less transparent compared to traditional statistical methods [10].

3.3 Resting state studies

Brain activity showing synchronized low-frequency signals (0.01-0.1 Hz) observed in resting-state functional connectivity was first demonstrated in [33]. Resting-state captures brain function when subjects are not focused on a task and reveals brain networks involved in *top-down* processing. These networks mainly include the DMN and dorsal attention network [33, 34], with minimal insights to the source of these triggers and hence termed ‘mind-wandering’.

As reviewed in [35, 36], resting-state analysis includes Time-Frequency Analysis (TFA), regional homogeneity, seed-based analysis, ICA, clustering, graph theory, and multi-band functional connectivity approaches. Further, deep learning based approaches [30] have also been applied for analysing resting state fMRI.

3.4 Graph signal processing studies

Graph theory efficiently assesses brain network states, modeling inter-relationships between brain areas via edges and nodes using various metrics. Previous studies have applied graph theory to identify measures of neurological and psychiatric disorders [37, 38], emotional brain states, and task-aware effective brain connectivity [26]. However, it hasn’t been utilized to study empathy-specific regions to the best of our knowledge.

In brain signal analysis, GSP has emerged as a powerful tool with diverse applications, including filtering brain activity using graph spectral modes [39] and signal decompositions [40]. GSP offers the advantage of extracting important structure-function relationships in the human brain by representing individual brain areas as nodes, enabling the analysis of small-worldness, modular organization, and highly connected hubs.

In functional brain connectivity analysis, approaches such as distance-based and Pearson’s correlation-based methods, as employed in [40] and [9], have been commonly utilized. Previous methods relying on smoothness assumptions, like those described in [41], have been outperformed by sparsity-based approaches.

Comparing with existing studies utilizing sparse representations. the approach in [42] focuses on learning task-aware effective brain connectivity using Graph Neural Network (GNN)s, where subject-specific functional connectivity networks are simultaneously computed for a group of subjects, regularized by group sparsity. In contrast, this work computes subject functional connectivity networks independently with individual node-domain sparsity constraints, maintaining subject-specificity and enabling subject-based analysis.

Unlike [43], which proposes a method for metric learning with spectral graph convolutions emphasizing spectral sparsity, this work imposes node-domain sparsity constraints, promoting the contrast of node-domain and spectral constraints. Furthermore, unlike the work in [44], which explores localization and temporal coherence in resting state paradigms, this study investigates sparse graph representations for task-based data, demonstrating versatility in addition to resting state scenarios.

In contrast to prior research utilizing GNN [26] and Graph Convolutional Network (GCN) [27] for task-based problems, this work focuses on GSP and graph learning based methods to model brain dynamics. Unlike densely connected graphs and convolutional operations commonly found in GNN and GCN approaches, this work prioritizes dynamic and sparse functional connectivity patterns, particularly in the context of studying empathy-related brain activity. GNNs and GCNs typically operate by propagating information across nodes in the graph to learn node embeddings or make predictions based on graph-structured data. While GNNs and GCNs have shown effectiveness in tasks such as node classification and graph-level prediction, they may not explicitly capture the deeper interactions and temporal dynamics relevant to empathy-related brain activity analysis.

This work extracts meaningful graph connectivity patterns directly from the data using optimization methods, distinguishing our approach from studies primarily employing GSP for task-oriented applications. This approach allows for a more flexible and adaptive analysis of brain connectivity, although it is important to consider the sensitivity of GSP to parcellation strategy and node specification when interpreting the results.

Chapter 4

fMRI data processing pipeline

4.1 Introduction

This chapter introduces a novel signal processing pipeline specifically designed to extract functional connectivity networks from fMRI data. The pipeline encompasses a series of pre-processing steps and leverages windowed graph learning techniques, with the ultimate goal of analysing secondary metrics extracted from the generated functional connectivity networks in the absence of a concrete ground truth network.

Most of the existing work involve pre-processing the raw fMRI BOLD signals with motion correction, coregistration to existing templates and data normalization [37–40, 45]. Subsequently, the data is directly used for graph inference tasks. However, without employing statistical methods like ICA (Independent Component Analysis), the presence of task-specific activations in a region can be obscured by various types of external (e.g., scanner noise) and internal (e.g., breathing, heartbeat) noises.

Moreover, in cases where regions are large, activations may not be uniformly distributed across the region but localized in specific sub-parts, potentially distant from the region's center. In such scenarios, existing approaches may struggle to accurately capture targeted activations, either by selecting an incorrect set of voxels (around the region's center) or by averaging out the activations across the entire region. In both the mentioned cases, the targeted activations may not be captured efficiently, leading to erroneous inferences.

This calls the need for denoising and voxel-level activation analysis for a more efficient and localized activation capture. The pipeline (shown in Figure 4.1) begins with normalization and high-pass filtering to improve data quality. Phase-based voxel clustering is then employed to reduce loss of activations due to out-of-phase voxels, capturing the activations better. Graph learning techniques, including Pearson-coefficient, node-distance, sparsity-based, and smoothness-based methods, are integrated to construct functional connectivity networks.

The pipeline and the subsequent analyses (detailed in Chapter 5 and Chapter 6) were run on an NVIDIA RTX 3050Ti GPU using MATLAB and Python code.

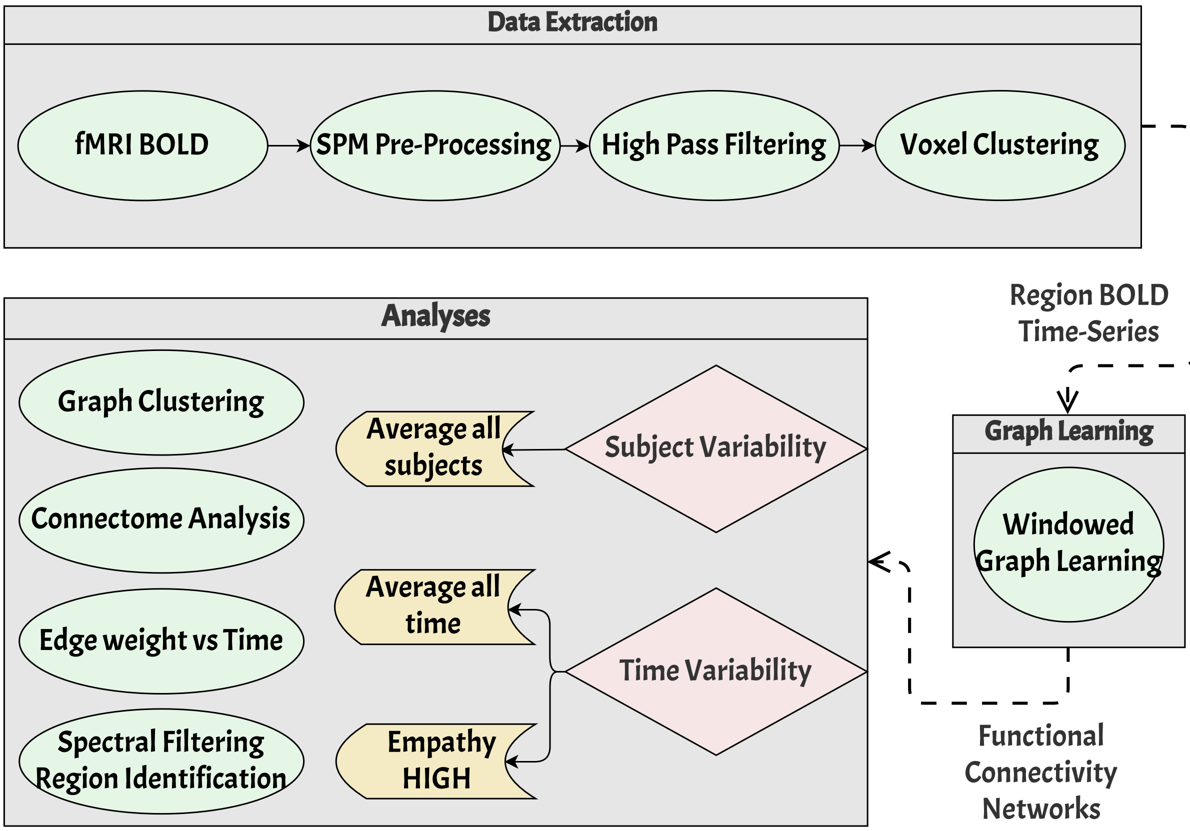

Figure 4.1 Pipeline used for fMRI BOLD signal functional connectivity analysis

4.2 Contributions

Some features and contributions of this pipeline are listed here.

- The pipeline uses raw fMRI BOLD signals from all voxels from chosen regions in the brain and modularizes the data extraction from voxel-level to region-level and finally extracts functional connectivity networks in a windowed manner.
- The pipeline involves utilization of optimization problems to obtain functional connectivity matrices from data over time-windows.
- The pipeline performs denoising using high-pass filtering and phase-based voxel clustering to remove misleading noise from raw fMRI BOLD data.
- Statistical methods like ICA are not used, ensuring the subjectivity of the analysis is not lost.
- Multiple analyses like the graph clustering over time, edge-weight dynamics and connectome-network analysis are included to analyse secondary metrics from the obtained graphs.

4.3 Data Extraction

The following subsections provide details of the data extraction module of the pipeline.

4.3.1 SPM-12 pre-processing of fMRI data

Pre-processing raw BOLD signals is a crucial step in fMRI data analysis, as it helps to remove noise and artifacts and extract meaningful information from the data. Pre-processing steps, such as slice-timing correction, motion correction, template-based normalization, and spatial smoothing, are typically applied to the raw fMRI data to improve the quality of the data.

The fMRI data were analyzed with Statistical Parametric Mapping (SPM)12 toolbox [46] running on MATLAB R2019a. Spatial pre-processing steps include: realignment (realigned to the mean image), coregistration (to each participant's individual T1 structural scan), segmentation (segmentation into grey, white matter and cerebrospinal fluid tissues) and template-based normalization (normalized to the Indian Brain Templates [47]). The slice time correction was avoided as the Repetition Time (TR) was 2 seconds [48]. The head movement correction was applied with the maximum head motion of < 2 mm and $< 0.5^o$.

4.3.2 BOLD signal normalization and High-Pass filtering

In fMRI BOLD processing, denoising the data is important to remove artifacts, enhancing signal interpretability and the accuracy of subsequent analyses. This section outlines the BOLD signal processing steps involving normalization and high-pass filtering.

The raw BOLD signal undergoes normalization through mean-removal, followed by high-pass filtering of the time-series signal at each voxel. Normalization ensures better capture of simultaneous activations, particularly when the mean value of each region's time-series is biased and non-zero. By removing the mean, all signals are centered around 0 DC (DC refers to the amplitude of zero-frequency component in a signal), enhancing the ability to capture small variations and temporal coincidences in the signals.

As depicted in Figure 4.3 (top), the signals exhibit a wide range of DC levels, spanning from 0 to 1700. This variability makes it challenging to capture simultaneous activations accurately. Despite potential similarities in signal shape, differences in DC levels persist, leading to a loss of activation capture. Mean removal addresses this issue by centering the signals around zero, facilitating the detection of subtle variations. However, variance normalization is omitted to preserve the magnitude of activation in different regions.

Another BOLD signal processing step is high-pass filtering, which targets the removal of slow temporal fluctuations unrelated to neural activity. These low-frequency components, including scanner drift, physiological noise and subject movement noise [49], can mask neural activity and reduce the sensitivity

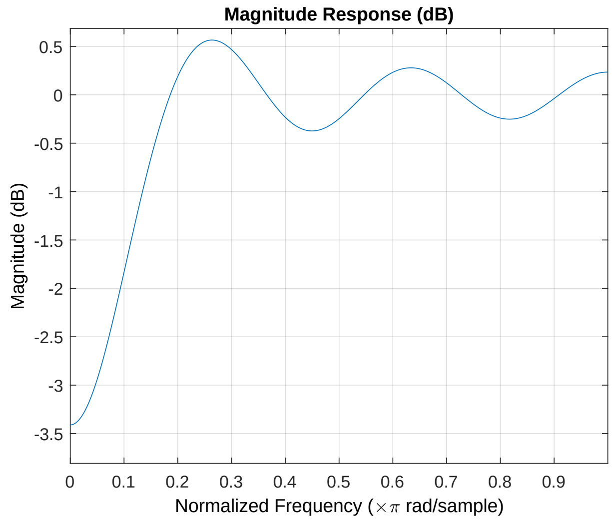

Figure 4.2 Magnitude response of the Least Squares FIR filter used for high-pass filtering

of the analysis to the effects of interest. By removing these low-frequency components using high-pass filtering, the quality of fMRI data can be improved. The removal of slow-moving signals from fMRI data can be particularly important in studies investigating the dynamics of brain networks [50], where the focus is on detecting and characterizing rapid fluctuations in neural activity. A Finite Impulse Response (FIR) Least-Squares high-pass filter, with a normalized cutoff of 0.043π rad/s ($\approx 0.05Hz$) is applied. An FIR filter is chosen to preserve phase information. The phase of the BOLD signals provides a notion of temporal synchronization, which is of interest in the further step of phase-based voxel clustering (detailed in Chapter 4 Section 4.3.3), as well as in specific analyses, detailed in Chapter 5 Section 5.7.3 and Chapter 6 Section 6.6.3.1.

The order of the filter is chosen as $N = 10$, the stop-band cutoff of $Fstop = 0.043$, the pass-band cutoff of $Fpass = 0.051$, the stop-band weight of $Wstop = 0.5$, pass-band weight of $Wpass = 1$ and density factor of $dens = 20$. It was generated using the filterDesigner tool of the Signal Processing Toolbox 9.0 in MATLAB R2023a. The magnitude response of the designed filter is shown in Figure 4.2. Further, after applying the filter over the time-series signal at each voxel, Figure 4.3 demonstrates the importance of high-pass filtering by illustrating improved neural activation capture compared to raw BOLD signals. The filtered time-series signal at one voxel from each of the regions chosen for an empathy-based study (detailed in Chapter 5) is shown.

4.3.3 Phase-based voxel clustering

A voxel represents a small three-dimensional parcellated portion of the brain. Voxel clustering aims to reduce flattening of activations due to out-of-phase voxels, thereby facilitating meaningful analysis at the regional level.

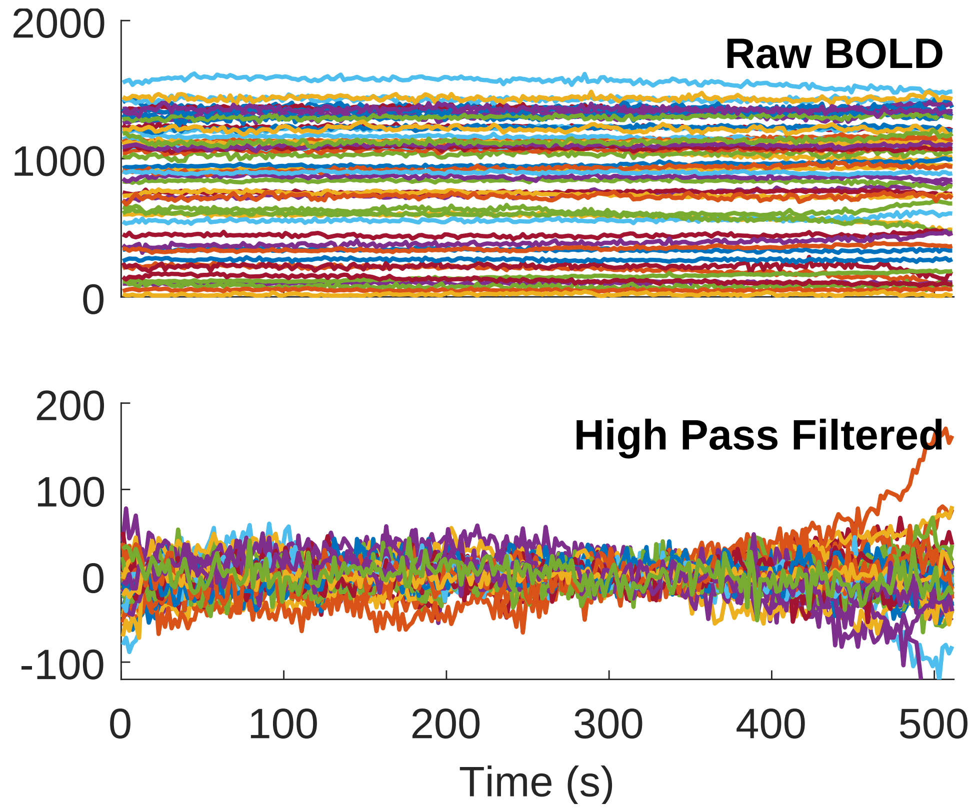

Figure 4.3 The raw BOLD and high-pass filtered BOLD signals at all the brain regions considered

Voxel clustering involves grouping voxels with similar activation patterns to obtain a representative signal for each brain region [51]. The phase component of the time-series signal at each voxel is chosen as the metric to compare similarity between voxel time-series, as the activation pattern is captured best in the phase component. Clustering on such a similarity metric ensures the voxels in a cluster posses similar phase components.

The phase of each voxel's time-series signal is obtained using Discrete Fourier Transform, and K-means clustering is applied to group voxels with similar phase patterns. The K-means clustering algorithm partitions the voxel time-series data into K clusters, where K is predefined. Each cluster represents a group of voxels with similar activation patterns. The algorithm iteratively assigns voxels to clusters based on their similarity to cluster centroids, aiming to minimize intra-cluster variance. The value of K is chosen as 3. This choice is made considering three states of voxels during a task - 1) task-specific activation state, 2) baseline resting state and 3) transitional or mixed state.

Following clustering, a post-clustering selection criterion is applied to choose the most representative voxel cluster for each brain region. This criterion typically involves selecting the cluster with the least intra-class variance, ensuring the selection of coherent signals while rejecting out-of-phase voxels. This

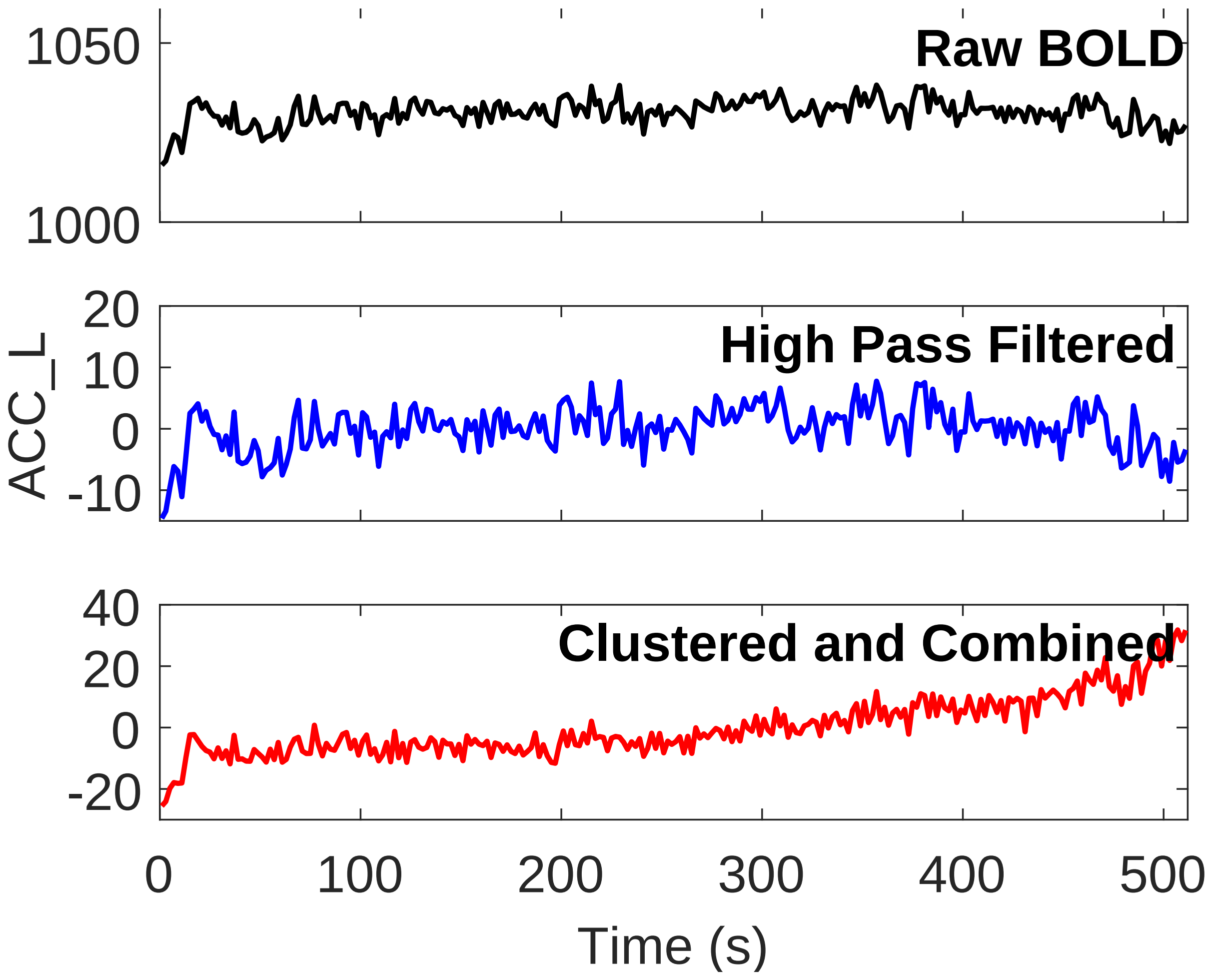

Figure 4.4 The progress in each step of the pipeline in processing the signal from raw BOLD to voxel-level combined BOLD

choice ensures that task-specific activations are preserved and can be better captured, followed by simple average performed over the selected voxels' time-series to obtain region-level time-series.

4.4 Region BOLD time-series

So far, the pipeline focused on BOLD signal processing. Figure 4.4 illustrates the current status of the pipeline's progression for an empathy-based task (detailed in Chapter 5). For visualization, at each stage of the pipeline, all voxels' time-series in Left ACC are combined to a single time-series through a simple average and subsequently analyzed. The impact of high-pass filtering is noticeable as it effectively eliminates slow variations in the signal attributed to factors such as scanner noise, breathing, and heartbeats—considered noise in the context of task-based analysis and thus rightfully discarded. The clustered and aggregated data visibly demonstrates that selecting voxels with similar phases enhances the capture of activations, preparing the data for the upcoming graph learning module.

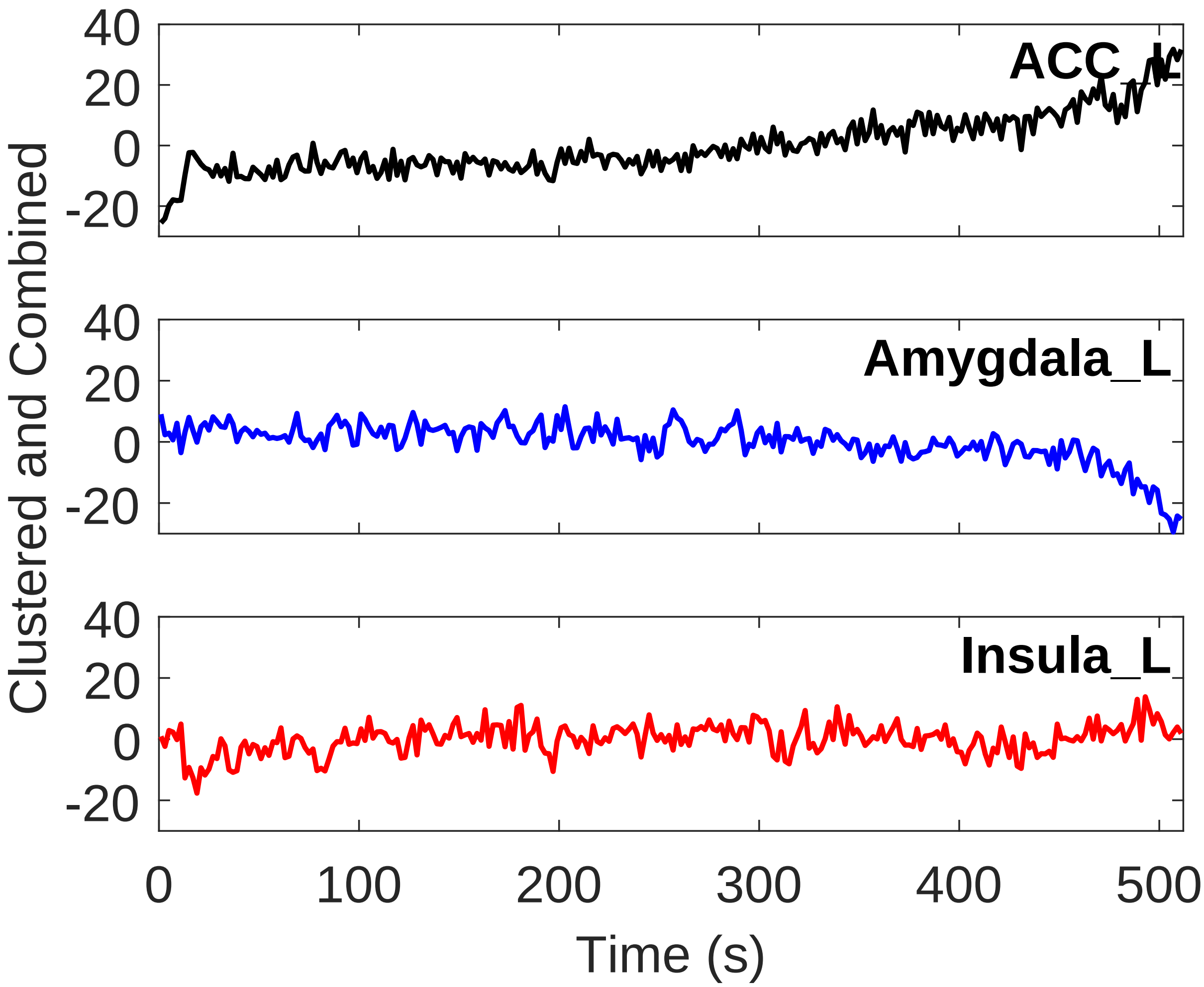

Figure 4.5 Region time-series signal for regions important for empathy processing like Insula (top), ACC (middle) and Amygdala (bottom)

Figure 4.5 shows the region time-series signal for regions important for empathy processing like Insula, ACC and Amygdala.

Subsequently, the upcoming module will involve the extraction of functional connectivity networks from the processed BOLD signals ($\mathbf{X}$). The data matrix $\mathbf{X}$ used in the graph learning module is an $N \times P$ matrix obtained by stacking $\mathbf{X}[n],\ n = 1, 2, ..., N$ which are the P dimensional signals (region level time-series) at each of the N regions.

4.5 Graph learning

Graph learning plays a crucial role in functional connectivity analysis, enabling the construction of networks that represent relationships between brain regions based on their activation patterns. This section explores application of graph learning techniques to learn functional brain connectivity.

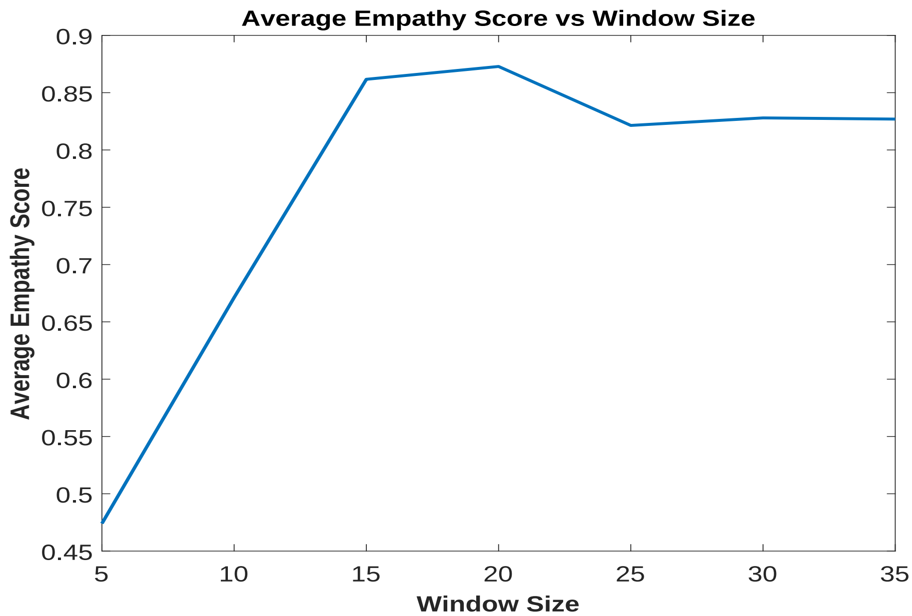

Figure 4.6 Variation of the accuracy of sparsity-based graph learning (here, the accuracy is measured as the average empathy score as detailed in Section 5.5.2) with respect to the window size

The graph learning process is conducted in a windowed fashion, taking into account the temporal dynamics of brain signals. Regarding the choice of the size of time window, [52] shows the hemodynamic response time of fMRI signals to be around 10 seconds, while the graph learning algorithms require at least 8-10 data points for obtaining a good accuracy [53]. With this knowledge a window size of 16 seconds was chosen for the study. Nevertheless, a comparative analysis is conducted across different window sizes varying from 5 to 35 seconds. Figure 4.6 shows the variation of the accuracy of sparsity-based graph learning (here, the accuracy is measured as the average empathy score as detailed in Section 5.5.2) with respect to the window size. It can be seen that the ideal choice of window size ranges above 15 seconds, after which the average empathy score plateaus. To maintain a considerable temporal resolution, the window size is chosen to be 16 seconds as the average empathy score remains approximately constant after 15 seconds. Windowing is executed in a sliding manner, with a stride of one sample, ensuring continuous coverage of the signal. Additionally, a non-windowed approach is included, where all the data samples are utilized for graph learning.

Utilizing multiple samples for learning is essential as a single time instant may not capture the full range of stochastic properties inherent in the signal [54]. By considering multiple samples, various stochastic properties of the time-series signal like state-dependent dynamics (like wakefulness, arousal, attention) and the hemodynamic response variability can be accounted for, aligning with the assumptions made by graph learning methods during the learning process.

Throughout all the graph learning methods and all the analyses to be discussed in further chapters, undirected, weighted graphs with no-self loops are used, making the graph Laplacian and the graph adjacency matrices symmetric.

Four graph learning techniques are employed to extract functional connectivity networks from the processed BOLD signals.

4.5.1 Pearson-coefficient

Pearson-coefficient-based graph learning [9] method models the node signals as random variables and finds the Pearson-correlation-coefficient between signals at every node pair. For P dimensional signals, the Pearson-correlation-coefficient between the signals at nodes n and m is given as

$$\rho(\mathbf{X}[n], \mathbf{X}[m]) = \frac{\sum_{p=1}^{P} \left(\mathbf{X}_p[n] - \mu_{\mathbf{X}[n]}\right) \left(\mathbf{X}_p[m] - \mu_{\mathbf{X}[m]}\right)}{(P-1)\sigma_{\mathbf{X}[n]}\sigma_{\mathbf{X}[m]}} \tag{4.1}$$

where, $\mathbf{X}_p[n]$ is the pth element of the signal at node n, $\mu_{\mathbf{X}[n]}$ and $\sigma_{\mathbf{X}[n]}$ are the mean and standard deviation of the time-series signal $\mathbf{X}[n]$. This is directly used in the adjacency matrix construction by setting the non-diagonal entries as $\mathbf{A}_{nm} = |\rho(\mathbf{X}[n], \mathbf{X}[m])|$, since $\rho(.) \in [-1, 1]$, and zero in the diagonal entries. Each graph signal is considered a random variable overlaid on the graph.

4.5.2 Node-distance

Node-distance-based graph learning [8] method computes the distance between the signals associated with every pair of nodes. The edge-weight ($\mathbf{A}_{nm}$) between the nodes n and m is then defined as

$$\mathbf{A}_{nm} = e^{-\frac{d_{nm}^2}{\sigma^2}}, \quad d_{nm} = ||\mathbf{X}[n] - \mathbf{X}[m]||_2 \tag{4.2}$$

where, $\mathbf{X}[n]$ and $\mathbf{X}[m]$ represent the graph signals at nodes n and m respectively, $||\cdot||_2$ represents the ℓ_2 norm of a vector, σ is a hyperparameter which controls the magnitude of weights generated. The choice of hyperparameters is provided further in Section 4.6. It is important to note here that the 'distance' referred to in the name of the method is not related to the anatomical distance between the regions, and is related to a distance-based metric between the signals at the two regions.

4.5.3 Smoothness

Smoothness-based graph construction method [55] learns a graph such that the given graph signals tend to be smooth on the learnt graph. It solves the following optimization problem

$$\{\hat{\mathbf{L}}, \hat{\mathbf{Y}}\} = \min_{\mathbf{L}\in\mathcal{L}, \mathbf{Y}} \frac{1}{2}||\mathbf{Y} - \mathbf{X}||_F^2 + \alpha \operatorname{Trace}\{\mathbf{Y}^T\mathbf{L}\mathbf{Y}\} + \beta\, ||\mathbf{L}||_F^2 \tag{4.3}$$

where, $||\cdot||_F$ denotes the Frobenius norm of a matrix and $\mathbf{L}$ is the graph Laplacian matrix. In (4.3), the first term represents data fidelity, which guarantees that the learnt data ($\mathbf{Y}$) closely approximates the observed data ($\mathbf{X}$), the second term represents the smoothness of the data and the third term ensures the entries of the Laplacian are small.

In 4.3 and 4.4, $\mathbf{L} \in \mathcal{L}$ imposes a constraint that a valid Laplacian is learnt, where $\mathcal{L}$ denotes the set of all possible valid Laplacian matrices. In order to ensure this, the following two constraints are added to the optimization problem: $\mathbf{L}.\mathbf{1} = \mathbf{0}$ and $\mathbf{L}_{ij} \leq 0 \,\forall\, i \neq j,\ i, j = 1, 2, ..., N$, which are the properties of a graph Laplacian matrix. Additionally, another constraint is added: $\text{Trace}\{\mathbf{L}\} = N$, which makes sure the trivial solution, that is, a null matrix is not obtained.

The optimization problem in (4.3) is not convex in both $\mathbf{L}$ and $\mathbf{Y}$. This is addressed by solving for each of these variables separately in an iterative manner [55] as follows:

$$\hat{\mathbf{L}} = \min_{\mathbf{L} \in \mathcal{L}} \ \alpha \,\text{Trace}\{\mathbf{Y}^T \mathbf{L} \mathbf{Y}\} + \beta \,||\mathbf{L}||_F^2 \,, \tag{4.4}$$

$$\hat{\mathbf{Y}} = \min_{\mathbf{Y}} \ \frac{1}{2}||\mathbf{Y} - \mathbf{X}||_F^2 + \alpha \,\text{Trace}\{\mathbf{Y}^T \mathbf{L} \mathbf{Y}\} \,. \tag{4.5}$$

The hyperparameter α governs the emphasis on smoothness, influencing the overall balance in the optimization process, while the hyperparameter β dictates the magnitude of entries in the Laplacian matrix.

4.5.4 Sparsity

Sparsity-based graph learning [56] tries to explain the signal at a given node using a sparse linear combination of signals at all the other nodes. Specifically, it solves an optimization problem for each node to extract its sparse connections which is converted into the adjacency matrix. For node n, the edge-weights $\boldsymbol{\beta}_n \in \mathbb{R}^{N-1}$ from node n to all the other nodes $m = 1, 2, ..., n-1, n+1, ..., N$ are estimated by minimizing the following objective function

$$\hat{\boldsymbol{\beta}}_n = \min_{\boldsymbol{\beta}_n} \ ||\mathbf{X}[n] - \mathbf{X}_n^T \boldsymbol{\beta}_n||_2^2 + \lambda \,||\boldsymbol{\beta}_n||_1 \tag{4.6}$$

where $\mathbf{X}_n$ is the data matrix of all the nodes except node n and $||\cdot||_1$ represents the ℓ_1 norm of a vector. The first term in the objective function ensures that the signal at node n is well described by the chosen neighbors whereas the second term promotes sparsity of connections. λ is a hyperparameter which controls the sparsity of the learnt edge-weights. The problem (4.6) can be solved using the LASSO algorithm [57]. Since the solution generally does not provide a symmetric adjacency, it is obtained by performing

$$\mathbf{A} = \sqrt{\mathbf{B}\mathbf{B}^T} \tag{4.7}$$

where $\mathbf{B}$ is the non-symmetric adjacency constructed using $\boldsymbol{\beta}_n$ for all nodes n.

4.6 Hyperparameter selection

Selecting appropriate hyperparameters is crucial for optimizing the performance of graph learning techniques in functional connectivity analysis. The efficacy of these techniques relies on the choice of hyperparameters, which may impact the resulting connectivity networks.

To determine the optimal hyperparameters for each graph learning technique, a systematic grid search methodology is employed. This approach involves systematically exploring a range of hyperparameter values and evaluating their performance using predefined metrics.

Through rigorous experimentation, optimal hyperparameter values are identified for each graph learning technique. These values are selected based on their ability to enhance the quality of extracted functional connectivity networks and improve overall analysis outcomes. The effectiveness of hyperparameters is evaluated using specific metrics tailored to assess the quality and robustness of functional connectivity networks.

For the node-distance-based approach, we find that setting the hyperparameter σ to 0.5 yields optimal results, evaluated based on the variance of edge weights preserved post-thresholding with 10^{-3}. Higher variance indicates better activation capture, thus identifying this hyperparameter choice as optimal. The smoothness-based method entails a 2D grid search for hyperparameters α and β, with optimal values of 0.25 and 9, respectively. Here, the chosen metric is the smoothness of the signal over the learnt graph, where graphs on which the signals are smoother indicate better hyperparameter choices. In the sparsity-based method, the hyperparameter λ is identified to be most effective at 2.5, with the number of edges in the graph serving as the metric. Smaller values of λ provide a dense graph, while higher values provide a very sparse graph. To strike the balance, the number of edges $|\mathcal{E}| \approx N$ is chosen, aiming for a graph that is informative yet not dense.

Chapter 5

Graph learning to understand empathy networks

5.1 Introduction

The exploration of empathy extends beyond mere observation, delving into the underlying neural mechanisms that drive this phenomenon. Understanding how the brain responds to empathetic experiences provides valuable insights into social cognition, emotional regulation, and interpersonal dynamics. Naturalistic stimuli like movies, or text narratives present an ecologically valid context to participants in an fMRI or EEG experiment, as real-life experiences are complex. Such stimuli can provide insights into brain networks, processing complex sensory information.

Using techniques like fMRI, experiments have revealed that the following constant but distributed brain areas [18–22], like the ACC (attributed to decision-making, social cognition, judgements and emotion regulation), Insula (emotion, self-awareness, introspection and critical for pain empathy), the Inferior frontal gyrus which supports a host of functions from language, memory, and cognitive driven judgements on other's emotional states, Amygdala (emotion processing especially fear), and the Superior temporal gyrus, Somatosensory cortex, the areas forming the default mode network (a resting state network) contribute to empathy networks in the brain.

Movies (short or full length) as stimuli in fMRI provide the context and the complex sensory input, which allows the viewer to form a scene-dependent empathy response, for analysis of the temporal dynamics of the brain regions [10–12]. The questions endeavoured to be answered by this preliminary study are: given the complexity of empathy brain networks and the multi-modal stimulus used, can methods be built to model whole brain dynamics reflecting the behavioral responses to the narrative? This study explores the application of various graph learning techniques to fMRI data for extracting region-level activation, analysing the dynamic functional connectivity of empathy-supporting brain regions within a whole-brain setting, and validating the findings by comparing emotional scale ratings with the graph clusters plotted over time.

In reference to this study, graph nodes represent brain regions, each node containing a time-series fMRI BOLD signal, further processed using the proposed pipeline before being used for learning the functional connectivity. We aim to learn the underlying brain functional connectivity among these regions from collective fMRI activation signals, particularly focusing on long-duration movie stimuli (it is a short movie, but from an fMRI standpoint, it is a long-duration movie). The learnt graphs' edge-weights quantify connectivity strength between different brain regions, allowing us to examine dynamic changes in edge-weights among different brain regions over time and variations in fMRI signals across the emotion scale. These graphs act as intermediate results, laying the groundwork for subsequent analyses and the derivation of more detailed outcomes.

This study presents novel contributions aimed at advancing the understanding of the neural correlates of empathy through fMRI data, which include -

- Proposing a unique signal processing pipeline incorporating high-pass filtering and phase-based voxel clustering.
- Utilization of graphs to model brain network states and investigate empathy-related brain activity in response to naturalistic stimuli, employing a sparsity-based graph learning approach.
- Comparison of the sparsity-based approach with existing methods, demonstrating superior performance in capturing relevant activations in empathy-related neural processes.
- Exploration of dynamic functional connectivity patterns and graph metrics, revealing alignment with the emotion scale (detailed in Chapter 5 Section 5.2) and highlighting key brain regions associated with empathy.
- Examination of edge-weight dynamics and variations between specific brain regions, indicating the effectiveness of the sparsity-based approach in identifying influential nodes and capturing temporal dynamics.
- Application of GFT for isolating task-specific regions using spectral-domain band-pass filtering, enabling the analysis of spectral filtering-based patterns and highlighting contributions from key brain regions across different stimulus intervals.

The results were analysed using codes written in MATLAB and Python on an NVIDIA RTX 3050Ti GPU. The codes are available online [58].

5.2 Data acquisition and pre-processing

The data used for the study was obtained from the Cognitive Sciences Lab, IIIT Hyderabad. The dataset was collected by Mohit, under the supervision of Kavita Vemuri.

Sixteen healthy subjects (9 male and 7 female) participated in this study. For the preliminary analysis performed in this work, 14 participants' data were considered. The consent form mentioned that two short movie clips of 8 minutes 45 seconds will be shown in the scanner. Additionally, as a part of the consent form and pre-scanning instruction, the experimenter informed the participant that they could quit the experiment at any time without any penalty. The human ethics committee of the Institute (Institutional Review Board (IRB)) approved the study, and all subjects provided a written informed consent. They received Rupees (Rs).1,500 ($18) in compensation for their time.

There were two short feature films used for the analysis: An Egyptian short film titled “These Times” (M1) and a Czech live action short film titled ”Most”, re-titled ”The Bridge” (M2). The story-line for both the movies and the plot for the emotion contagion scale are provided in Appendix A, at the end of this chapter. The movies were edited to run for 8 minutes 45 seconds approximately. The rationale for considering the non-local language movies was - a) The movies had actors who did not have same ethnicity as the participants, to control for intra-cultural biases arising from economic status, caste, language, and physical characteristics and b) the direction was concise and had very poignant instances of change in narrative.

Along with the movies, resting state data was also collected for a duration of 3 minutes. The total number of scans was 262 for M1 and 242 for M2. The total number of scans for the resting state data was 90. Additionally, 40 participants with similar backgrounds participated in a survey to dynamically scale the movies on emotional context (refer to Appendix B), which acts as the ground truth in all the studies discussed in Chapter 5 and Chapter 6. The emotion scale shown in Appendix B is at a sampling rate of 1Hz (1 sample per second), but the TR for the fMRI scan was 2 seconds (sampling rate of 0.5Hz). Thus, for all the analyses using the emotion scale, the original scale had been downsampled by a factor of 2, by rejecting alternate samples. Further, mean removal and scaling had been performed for visualization.

5.3 Regions considered and choice of ATLAS

The selection of brain regions was conducted using the AAL Atlas, encompassing a total of 54 bilateral regions (27 on each side of the brain). The chosen regions were strategically picked to ensure comprehensive coverage, particularly focusing on frontal areas. Emphasis was given to empathy-specific regions such as the Insula, ACC, and Triangularis. In addition to these targeted regions, a broader set was considered to cover the entire brain while avoiding redundancy.

It is worth noting that all 90 regions from the AAL Atlas were not included in the study, as the chosen regions were curated to provide ample representation across the frontal, parietal, occipital, and temporal lobes, ensuring a well-rounded coverage of the entire brain. This selection not only serves the purpose of studying empathy-associated regions but also optimizes computational efficiency by avoiding unnecessary redundancy, thereby expanding the practical applicability of the analysis. The list of regions chosen for the analysis has been provided in Appendix C.

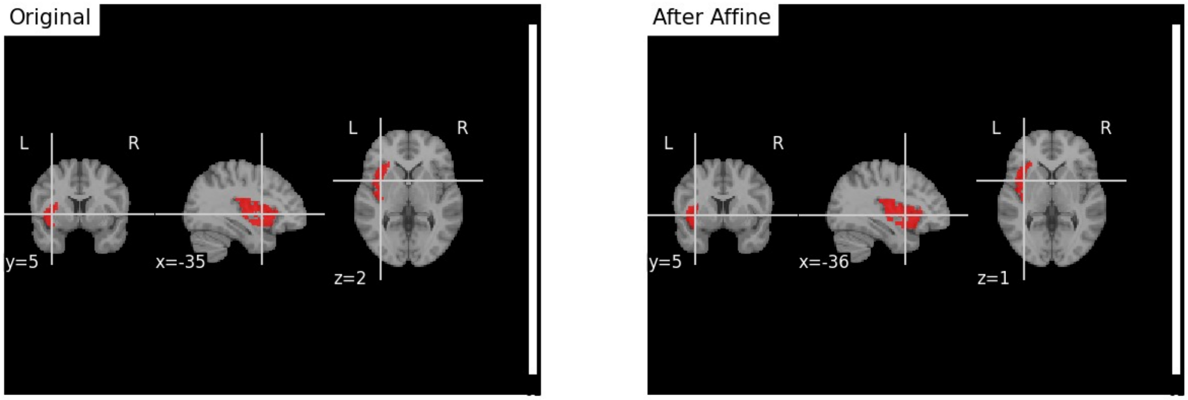

Figure 5.1 Masks for Left ACC before and after the resizing using affine transform

5.4 Applying masks on the data

The process of region-based voxel time-series extraction begins with the acquisition of masks from the AAL3 Atlas using the SPM12 toolbox in MATLAB. These masks correspond to specific brain regions of interest. Subsequently, to ensure compatibility with the dimensions of the fMRI data, which are typically $79 \times 96 \times 32$ images, the extracted masks undergo resizing using an affine transform associated with them. This affine transform applies a combination of translation, rotation, scaling, and shearing operations over the mask. This resizing procedure, executed using the Nilearn and Nibabel libraries in Python, adjusts the dimensions of the masks from their original size of $91 \times 109 \times 91$ to align with the data dimensions. Figure 5.1 shows the masks for Left ACC before and after resizing with the affine transform.

Following resizing, the scaled masks are applied to the fMRI data. This application enables the extraction of time-series data for all voxels within each region of interest. Given that the acquired masks are binary, indicating voxels that belong to a particular region, element-wise multiplication is performed between each mask and the each of the 3 Dimensional (3D) slices (one time instant) of the 4 Dimensional (4D) (whole time-series) fMRI data.

Subsequently, the entries in the resulting matrix where the mask is non-zero are consolidated region-wise into two dimensional matrices. This consolidation step effectively compiles the time-series data for all the voxels in the given region, facilitating further analysis. This entire process is iterated across all 54 regions of interest.

5.5 Preliminaries

5.5.1 Graph Clustering

In this work, multiple graphs corresponding to distinct time intervals are generated using the windowed graph learning. The objective of graph clustering is to reveal underlying temporal patterns within this set of graphs. This analysis uses hierarchical clustering with ward linkage [59]. Ward linkage is preferred over other hierarchical methods due to its ability to minimize within-cluster variance, leading to well-defined clusters that preserve the hierarchical structure of the data. The method initializes with each data point as its own cluster, treating them as individual singleton clusters. Further, the algorithm iteratively merges clusters to minimize the increase in total within-cluster variance, resulting in a dendrogram that represents the hierarchical structure of the data [59].

This analysis flattens the adjacency matrix of each graph into an $N^2 \times 1$ vector, which are subsequently clustered over the entire time range. This clustering approach enables the categorization of graphs based on their inherent similarities, allowing the exploration of the temporal evolution of graph structures.

The specific interest in this work focuses on binary classification, aiming to differentiate between empathy-related and non-empathy-related graphs. To assess the efficacy of any graph learning algorithm in extracting functional connectivity, particularly concerning neural activations linked to empathy, the clusters are examined in relation to the emotion scale. As mentioned in Section 5.2, the emotion scale acts as a notion for ground truth to compare with and will be used similarly throughout this work.

5.5.2 Cross-correlation and empathy score

To evaluate the empathy levels of each subject against the ground truth, represented by the emotion scale, cross-correlation is chosen as the metric. Cross-correlation assesses the similarity between two signals by examining their alignment across various time shifts. In signal processing, it quantifies the resemblance between the shapes of two signals. By computing correlation coefficients at different time lags, cross-correlation indicates the degree of matching between the signals at different time points. This metric ranges from -1 to 1, where a value of 1 indicates a perfect match, 0 denotes no correlation, and -1 signifies perfect anti-correlation. The cross-correlation between signals $\mathbf{x}$ and $\mathbf{y}$ at time-shift τ is mathematically given as

$$CC_{\mathbf{xy}}(\tau) = \sum_{n=-\infty}^{\infty} \mathbf{x}[n]\mathbf{y}[\tau + n] \tag{5.1}$$

where $\mathbf{x}[n]$ denotes the $n - th$ sample of the signal $\mathbf{x}$.

Applied to time-series data, cross-correlation facilitates the evaluation of temporal alignment and synchronization between signals, providing a quantitative measure of the percentage match between their shapes. This proves particularly useful where the signals vary in absolute values, but are similar in shape, rendering it suitable for quantifying the 'empathy score'. In this work, 'empathy score' is defined as the percentage match of the temporal graph clustering labels with the emotion scale, which is calculated using the highest cross-correlation match between the two signals.

5.6 Analyses

The obtained graphs undergo further processing to extract essential metrics, considering two main dimensions: time and subjects. Temporal analysis is condensed into two distinct perspectives: 1) Averaging across all time points and 2) focusing on the time point with the highest emotional valence, labeled as 'emotion HIGH' (around 360-400 seconds interval in M1). In terms of subjects, the analysis is performed by averaging across all subjects. The analyses are performed over both the movies separately. The analyses include graph cluster labels, connectome-network analysis, edge-weight dynamics, region identification with processed BOLD signals (prior to graph learning), BOLD signal vs emotion contagion scale and region identification using spectral filtering, detailed further.

It is important to note that in all the analyses, due to the absence of any concrete ground truth of the functional connectivity networks, performance analysis has been done by comparing the emotion scale with secondary metrics extracted from the obtained networks, like graph cluster labels, edge-weight dynamics and regional graph signal values in spectral filtering.

5.6.1 Region identification with processed BOLD

Prior to the graph learning module, the pre-processed BOLD signals undergo an initial examination to identify regions associated with empathy. This involves extracting region-level time-series data utilized prior to the graph learning process. The time-series data is then cross-correlated with the emotion contagion scale to quantify the degree of similarity between the two signals. The cross-correlation metric is employed to determine the percentage match, ultimately revealing the top 5 regions exhibiting the highest correlation with the emotion scale.

The objective of this analysis is to compile a list of regions activated in accordance with the emotion scale, bypassing the need for functional connectivity learning. These results are later compared with the regions and connections highlighted through the functional connectivity analysis.

5.6.2 BOLD signal vs emotion scale

Prior to the graph learning module, the pre-processed BOLD signal amplitudes at each level in the Left Insula are regressed over the emotion scale values given at each time instant. The main objective of this analysis is to observe the spread of BOLD signal amplitudes across various emotion scale ratings to understand the importance of graph learning in providing a detailed perspective of empathy networks.

5.6.3 Graph clustering vs emotion scale

After generating graphs with the graph learning module, the graphs are clustered as detailed in Section 5.5.1. The current utilization of a binary clustering algorithm, which simplifies the identification of empathy presence at a given time instant, proves effective in discerning optimal graph learning methods for the specific stimulus, which is the primary objective of this analysis. The evaluation focuses on their ability to distinguish between empathy-related and non-empathy-related networks, aligning with the emotion scale.

This analysis further aims to identify the graph-based assumptions (like signal smoothness, sparsity) best suited for a naturalistic stimuli, which can be inferred from the optimal graph learning method identified. This aids in the formulation of informed decisions regarding the properties and assumptions applicable to brain signals, particularly concerning connectivity during an external stimulus. Subsequently, the empathy scores are generated and averaged across subjects as detailed in Section 5.5.2, identifying the most effective graph learning method.

5.6.4 Edge-weight analysis

This analysis comprises two distinct sub-parts: 1) Temporal evaluation of edge-weight between specific regions associated with empathy, and 2) analysis of edge-weight dynamics in relation to the emotion scale. After obtaining the graphs, the focus shifts to extracting the edge-weight between two regions and analysing its temporal dynamics.

5.6.4.1 Edge-weight dynamics of important edges

In this analysis, the simultaneous activation of two empathy-specific regions, as reflected in their edge-weights over time is investigated. From this analysis, the primary objective is to highlight the impact of sparsity-based approach over the others in capturing temporal coincidences in regional activations.

5.6.4.2 Edge-weight dynamics correlated with emotion scale

This analysis involves observing the dynamics of edge-weights for all possible connections within the obtained graphs. The objective is to identify the top 5 edges that exhibit the highest alignment with the emotion scale, facilitating the recognition of edges crucial to empathy. The alignment is quantified using the cross-correlation metric. This approach aids in comprehensively understanding the interplay between specific regions and identifying edges that strongly correlate with the emotion scale, thereby highlighting connections integral to an empathetic response.

5.6.5 Connectome-based network analysis

As a part of this analysis, edge thresholding is implemented on the obtained graphs, specifically focusing on the top N edges (where N is the number of nodes in the graph) while discarding the remaining ones. Further, the top 5 edges are highlighted in red. This process highlights networks within the brain, emphasizing significant and strong connections during distinct time intervals throughout the stimulus. The primary objective is to identify and compare the regions associated with the strongest edges resulting from diverse time-based analyses. This comparison becomes particularly vital as it enables us to contrast connectivity patterns and identify regions characterized by robust connections, differentiating between all-time-average and the emotion HIGH time-window.

5.6.6 Region identification with spectral filtering

This analysis delves into the GFT-based filtering method outlined in Section 2.1.2. Notably, the smoothness-based graph learning approach carries an inherent assumption of data smoothness across the learnt graph. Consequently, studying the spectral decomposition of data over such graphs may be less suitable, given that energy tends to concentrate primarily on the lower set of graph frequencies. In contrast, sparsity-based graph learning avoids such assumptions, making its spectral analysis an insightful exploration across various frequency bands.

This study specifically focuses on three bands: 1) the low-pass band (comprising the bottom one-third of the graph frequency spectrum), 2) the band-pass band (encompassing the middle one-third) and 3) the high-pass band (encompassing the upper one-third). As detailed in Chapter 3 Section 2.1.2, emphasis is placed on the band-pass band due to its capacity to concentrate on specific patches and sets of regions within the graph, in contrast to the broad coverage of the low-pass band or the deeper localization inherent in the high-pass band.

The procedure unfolds step-wise, commencing with the GFT applied over the graph signal at a chosen time window with respect to its corresponding graph. Given that the data is windowed for learning the graphs, the median of each data window is selected for the graph spectral analysis. Subsequently, band-pass filtering is executed by discarding the lowest one-third and highest one-third coefficients, retaining only the band-pass band. These coefficients are then utilized to perform an inverse GFT, transforming back to the node-domain signal.

The primary objective of this analysis is to scrutinize groups of regions associated with empathy-specific activations and analyse variations highlighted across different time-based analyses. Notably, this analysis extends beyond the realm of BOLD signal activations, capturing nuances attributable to the underlying graph structure. This multifaceted approach adds depth to the exploration of empathy-specific regions.

5.7 Results

A comprehensive analysis across different graph learning methods is performed using average empathy scores as the metric, which are the correlation percentages between graph clustering labels and the emotion scale, averaged across subjects. Section 5.7.3, reveals the performance of the sparsity-based method in aligning with the emotion scale, in both the movies. Consequently, further analyses are restricted exclusively to sparsity-based graph learning.

Further, results such as graph cluster labels and edge-weight dynamics are excluded from the results with the two broad time-based analyses as they require the whole time-series. On the other hand, the remaining analyses, such as connectome analysis and region identification with spectral filtering, undergo both the time-based analyses, and the outcomes for M1 are systematically presented in Table 5.1. All the analyses are performed for both the movies.

5.7.1 Region identification with processed BOLD signals

From this analysis, regions such as Left Fusiform Gyrus, Right Inferior Temporal, Left Inferior Temporal, Left Medial Orbital Frontal, and Left ParaHippocampal emerged when averaged across all subjects. Of particular significance are Left Fusiform Gyrus and Left ParaHippocampal, which are closely associated with empathy-related functions.

5.7.2 BOLD signal vs emotion scale

According to the scatter plot in Figure 5.2, most of the BOLD signal levels are clustered at lower emotion scale values and show higher variance. BOLD signal levels for higher emotion scale values on the other hand are spread sparsely implying that the subjects did not show higher emotional response for the parts of the movie rated higher in emotion scale provided by the independent scorers. The boxplot in Figure 5.3 shows higher dispersion but comparable medians of the BOLD signals for emotion scale values less than 0.6, while for the values equal to or more than 0.6, the dispersion is less but BOLD median values show a random pattern across subjects i.e. they are not comparable. The sparse distribution and lower dispersion for higher emotion scale values imply smaller range for BOLD signals. We can conclude from the two figures that a simple BOLD level analysis is not sufficient to make inferences regarding empathy traits of individuals. This lays ground for the importance of connectivity based analysis techniques.

5.7.3 Graph clustering vs emotion scale

The sparsity-based approach consistently captures variations in the emotion scale as shown in Figure 5.4, with all participants demonstrating alignment of over 80% with the emotion scale. When subject responses are averaged, the distance, Pearson's correlation, smoothness, and sparsity-based methods

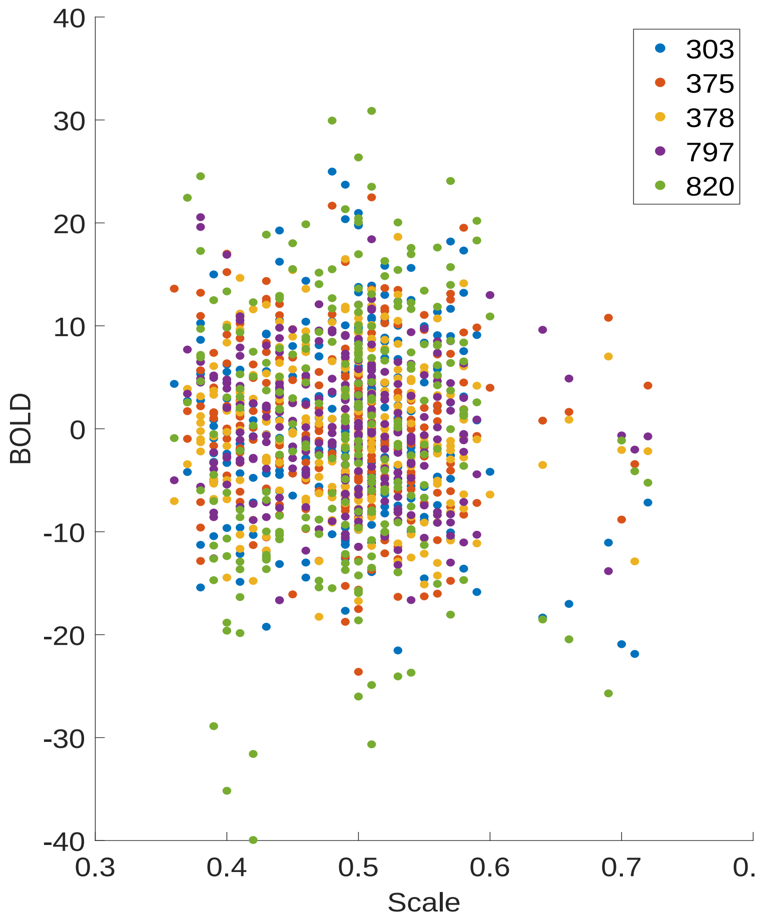

Figure 5.2 Scatter plot of BOLD signal in the Left Insula for 5 subjects (shown in the legend) vs emotion contagion scale for M1

exhibit 80%, 72%, 80%, and 88% match with the emotion scale, respectively. Figure 5.4 (top) illustrates the temporal variation of graph cluster labels using the sparsity-based method, averaged across all subjects overlaid on the emotion scale for M1.

A notable finding is that, up to the 180 seconds mark in the movie, the averaged graph clustering labels show limited correlation with the emotion scale. However, they become highly synchronized post 180 seconds. The above mentioned values are with respect to M1. Figure 5.4 (bottom) shows temporal variation of graph cluster labels using the sparsity-based method, averaged across all subjects overlaid on the emotion scale for M2, and it can be seen that similar to M1, sparsity-based approach is able to consistently capture emotion scale variations after 120 seconds, with an overall of 88% match.

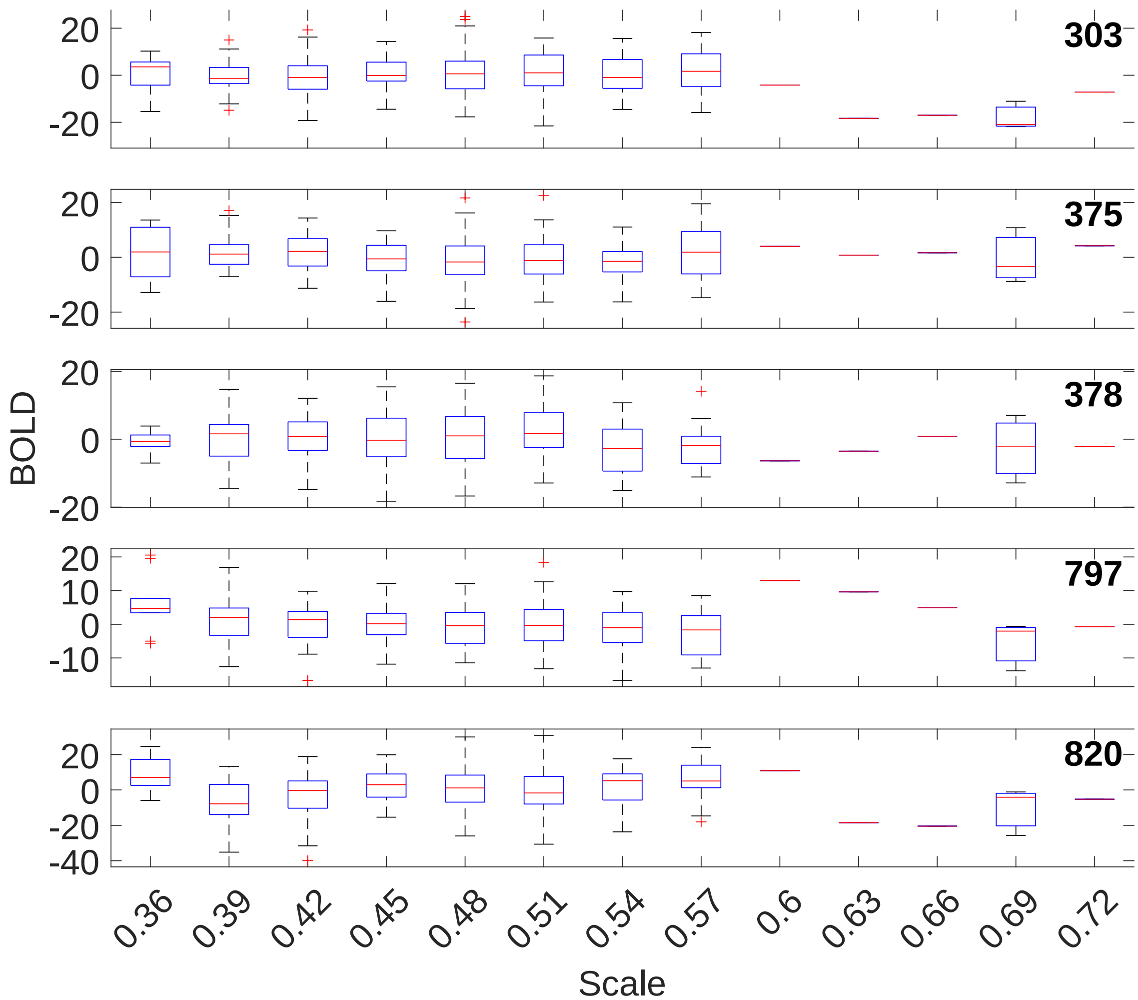

Figure 5.3 Boxplots of BOLD signal for all subjects vs emotion contagion scale

As a comparison with the existing methods, Figure 5.5 shows that other methods like distance, Pearson's correlation and smoothness-based approaches fail to capture temporal variations, with a lower match with the emotion scale, showing the ability of sparsity-based approach to capture activations better in a task-specific stimulus.

5.7.4 Edge-weight dynamics

In the analysis targeting the edge-weight dynamics between empathy-specific regions, the time dynamics of the edge-weight between Right Insula and Right Triangularis Frontal was analysed. Figure 5.6 compares different graph learning methods for a randomly selected subject. The distance-based method exhibits peaks around 250 seconds in the Insula-Triangularis connection for 10 out of 14 sub-

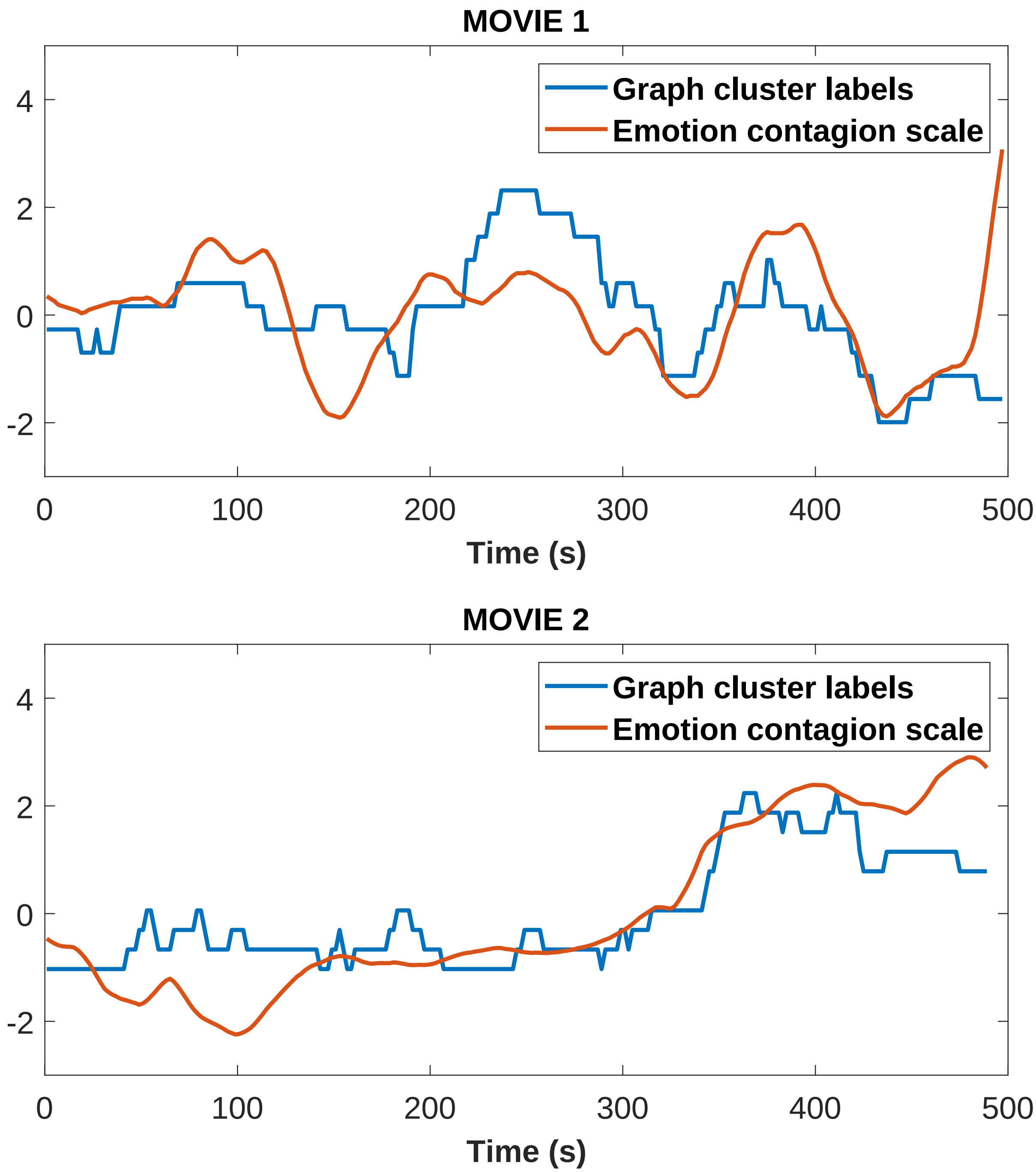

Figure 5.4 The subject-averaged graph cluster labels superimposed with emotion contagion scale plotted over time for M1 (top) and M2 (bottom) for the sparsity-based approach

jects, while the Pearson's correlation-based method lacks clear edge identification. The sparsity-based method identifies peaks around 250 seconds and 475 seconds in 11 out of 14 subjects, which aligns with the peaks observed in the emotion scale in Figure 5.4. Further, the smoothness-based method identi-

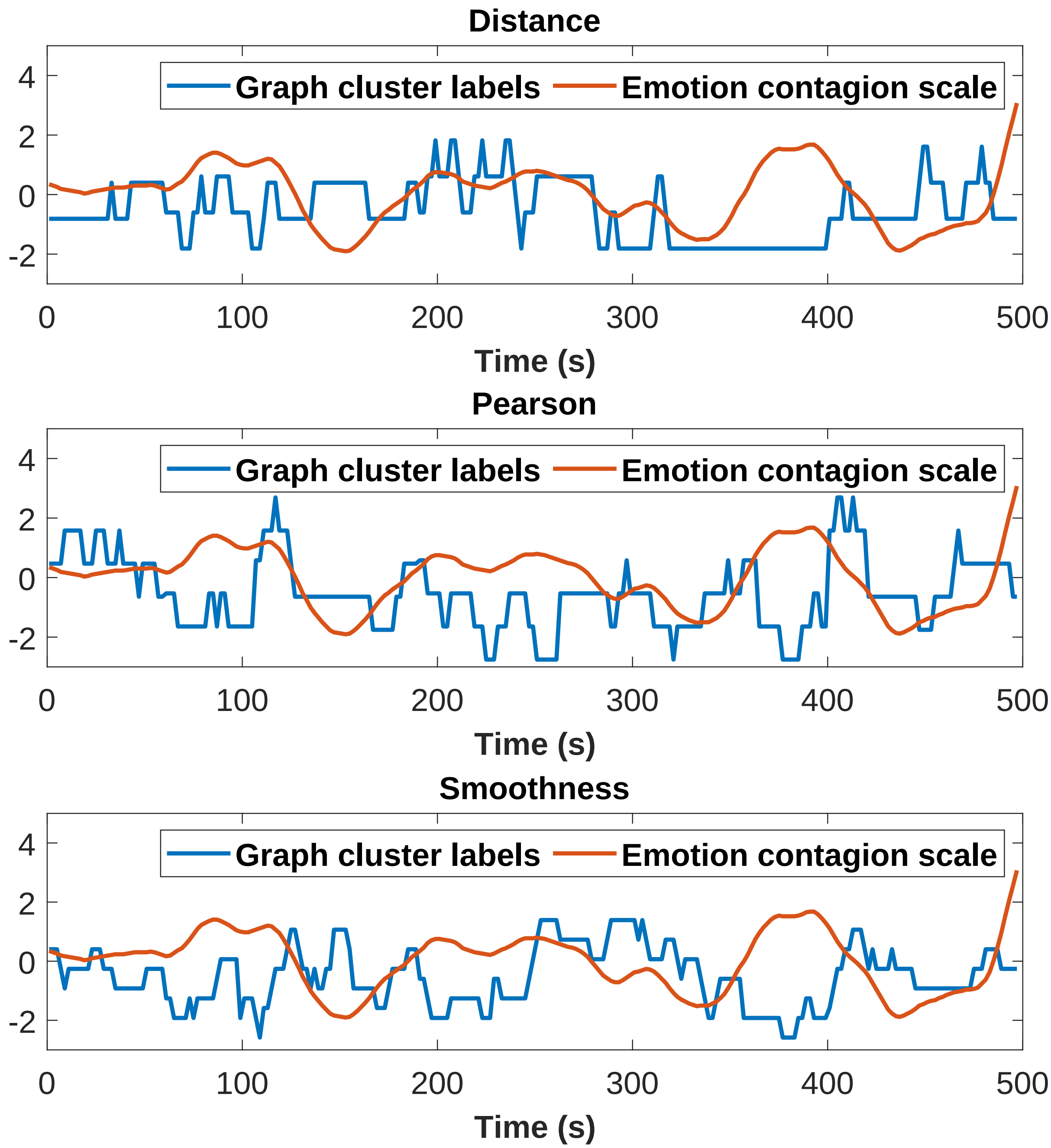

Figure 5.5 The subject-averaged graph cluster labels superimposed with emotion contagion scale plotted over time for distance-based (top), Pearson's correlation-based (middle) and smoothness-based (bottom) approach for M1

fies peaks around 50 seconds which may not be strongly attributed to an empathetic response. Figure 5.6 distinctly illustrates the susceptibility of Pearson's correlation-based approach to noise, resulting in noisy activations. This underscores the superior performance of the sparsity-based approach when dealing with a noisy, task-based stimulus, with activations in-line with the emotion scale.

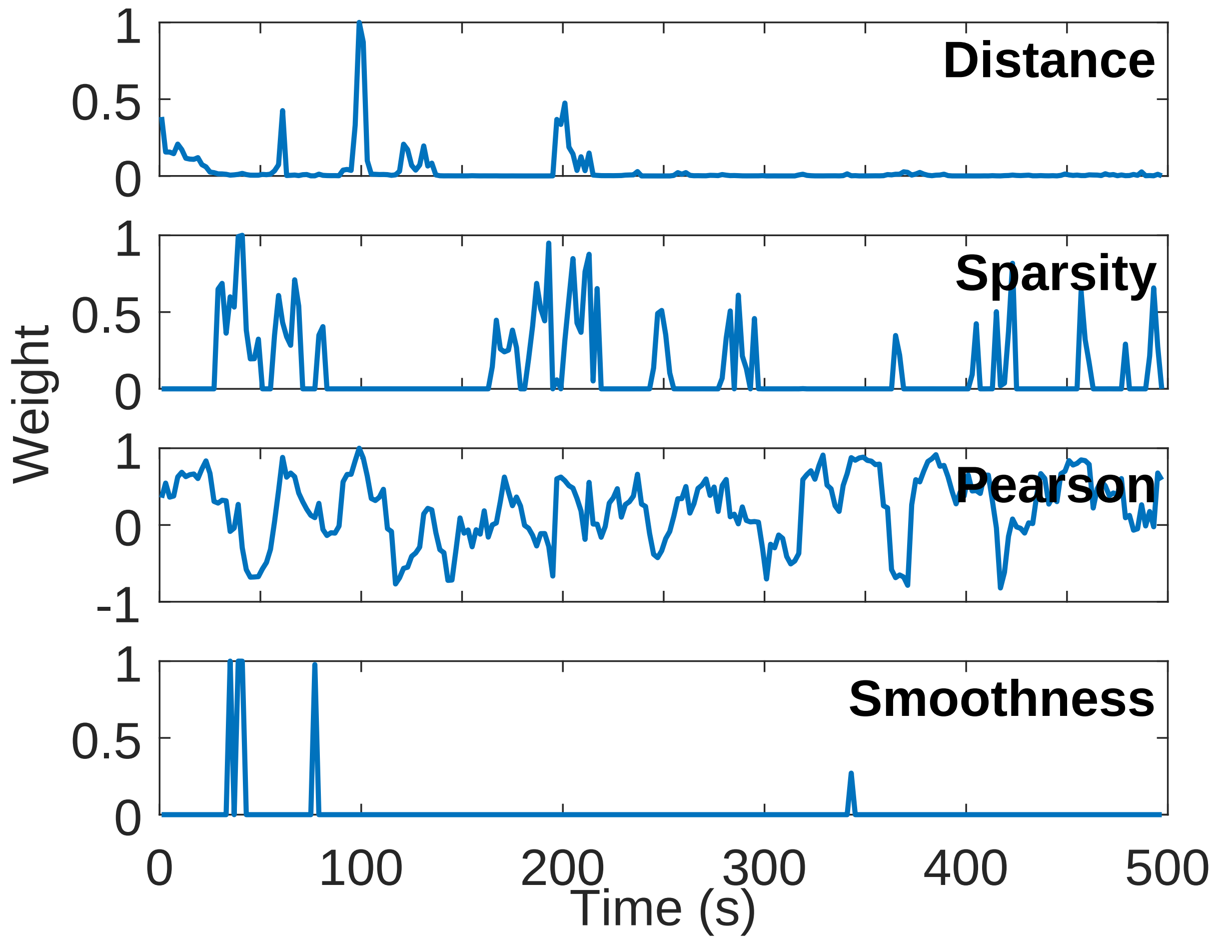

Figure 5.6 Edge-weight between Right Insula and Right Opercularis Frontal for one subject using all methods

In the analysis targeting edges with edge-weight dynamics most correlated with the emotion scale, several significant connections were identified. Averaging across all subjects revealed prominent edges, including Left Medial Superior Frontal ↔ Right Superior Frontal, Right Inferior Orbital Frontal ↔ Left Inferior Temporal, Left ParaHippocampal ↔ Left Inferior Temporal, Right Inferior Orbital Frontal ↔ Right Inferior Temporal, and Right Medial Orbital Frontal ↔ Right Inferior Temporal for M1.

5.7.5 Connectome-based network analysis

The listed networks comprise a collection of regions characterized by the strongest edges within the acquired graphs, as shown in Figure 5.7 and Figure 5.8. This selection is based on the top 5 edges (in magnitude), shown in red in the figures. The top N edges are also shown in the figures, in blue. The two regions associated with each of these edges are listed. In the context of connectome-based network analysis, specifically during the emotion HIGH interval, the regions Left Insula, Right Inferior Parietal, Left Thalamus and Right Amygdala consistently emerge. In the scenario of all-time-average

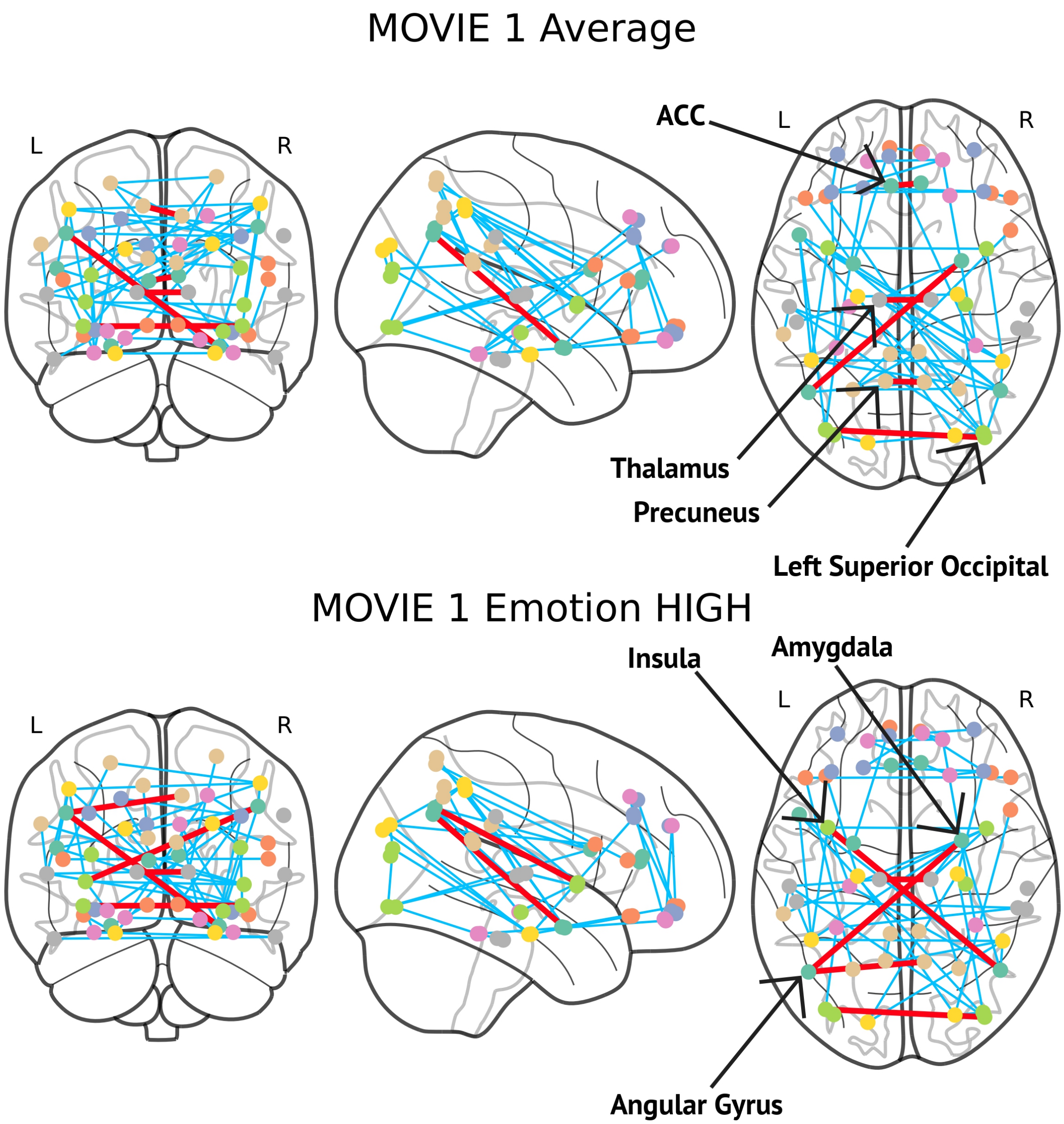

Figure 5.7 Connectome graph illustrating the networks learnt using sparsity-based graph learning. The significant nodes are labelled according to the AAL Atlas. The blue edges correspond to the significant top-N edges, and the red edges correspond to the strongest 5 edges in the graph Adjacency. It shows variation in networks obtained by averaging on all time (top) and during emotion HIGH interval (bottom) in M1

analysis, we observe bi-lateral connections being formed with the same region for both the movies, specifically between Left ACC $\leftrightarrow$ Right ACC, Left Thalamus $\leftrightarrow$ Right Thalamus, and Left Precuneus $\leftrightarrow$ Right Precuneus. During all-time-averaged analyses across both the movies, we observed that the edges between Right Amygdala $\leftrightarrow$ Right Angular Gyrus and Left Inferior Occipital $\leftrightarrow$ Right Inferior Occipital

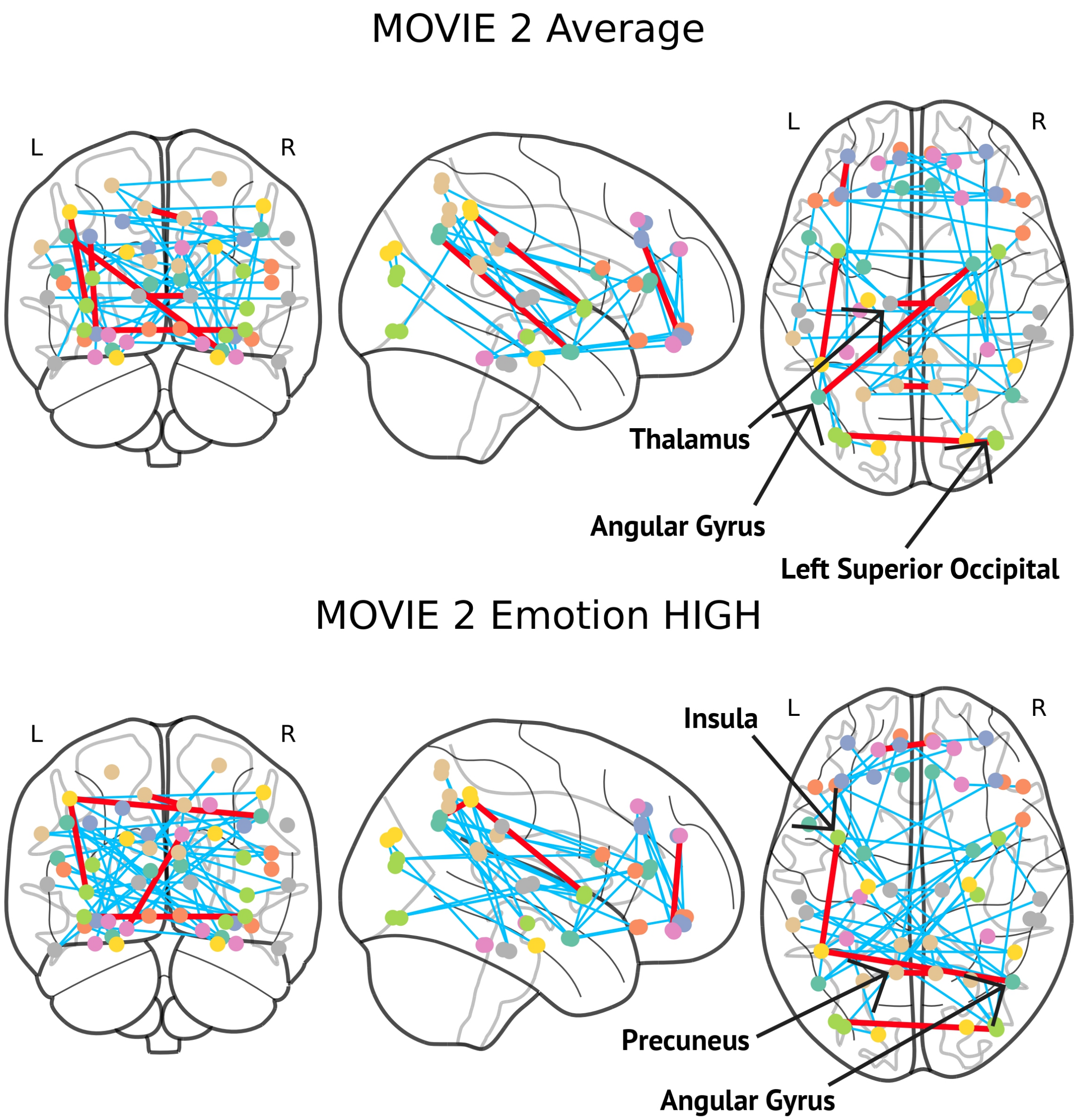

Figure 5.8 Connectome graph illustrating the networks learnt using sparsity-based graph learning. The significant nodes are labelled according to the AAL Atlas. The blue edges correspond to the significant top-N edges, and the red edges correspond to the strongest 5 edges in the graph Adjacency. It shows variation in networks obtained by averaging on all time (top) and during emotion HIGH interval (bottom) in M2

prevail. During the emotion HIGH interval, in both the movies, the edge between Left Inferior Occipital $\leftrightarrow$ Right Inferior Occipital is not present. Summarizing, across both the movies, during the emotion HIGH interval, the Insula, Amygdala and ACC and Angular Gyrus appear to have strong connections.

Analysis	Time	Average (Avg). on all subjects
Connectome - network	Avg. on all time	Left ACC $\leftrightarrow$ Right ACC, Left Thalamus $\leftrightarrow$ Right Thalamus, Left Precuneus $\leftrightarrow$ Right Precuneus, Right Amygdala $\leftrightarrow$ Left Angular Gyrus
	Emotion HIGH	Left Insula $\leftrightarrow$ Right Inferior Parietal, Left Thalamus $\leftrightarrow$ Right Thalamus, Left Inferior Occipital $\leftrightarrow$ Right Inferior Occipital, Right Amygdala $\leftrightarrow$ Left Angular Gyrus
Spectral filtering	Avg. on all time	Left Hippocampus, Right Angular Gyrus, Right Inferior Triangularis Frontal, Right Superior Frontal, Left Inferior Temporal
	Emotion HIGH	Right Amygdala, Right Insula, Right Thalamus, Left Angular Gyrus, Right Middle Orbital Frontal

Table 5.1 Summary of regions and networks identified through graph Fourier transform-based region identification and connectome-based network analysis for different empathy levels for M1

5.7.6 Region identification with spectral filtering

In contrast to the emphasis on edges in connectome-based network analysis, the spectral filtering-based approach facilitates the identification of regions across different graph frequency bands. Signals that have undergone spectral filtering are visualized over the graph, and the regions exhibiting the top 5 amplitudes are selected.

Specifically, during GFT-based filtering in the emotion HIGH (around 360-400 seconds in M1) time window, regions pivotal to empathy such as Right Amygdala, Right Insula, Right Thalamus, Left Angular Gyrus, and Right Middle Orbital Frontal consistently stand out for M1 as shown in Figure 5.10. These regions are recurrently highlighted across the top 5 amplitudes, underscoring their significance in capturing heightened empathy states. In contrast, during all-time-average analysis, distinctive regions, including Right Superior Frontal, Left Hippocampus, Left Inferior Temporal, Right Angular Gyrus, and Right Inferior Triangularis Frontal (Triangularis), emerge prominently, demonstrating shifts in neural activity associated with empathy states on an average across time.

Regarding M2, in the emotion HIGH time window (around 370-410 seconds in M2), common highlighted regions include Left Amygdala, Left Insula, and Right Insula, as shown in Figure 5.11, mirroring the observations from M1. Additionally, Left Fusiform Gyrus and Left Medial Orbital Frontal emerge as noteworthy regions uniquely emphasized during this period. In Figure 5.9, the filtered graph signal at each region is depicted on a colorbar for M1. The low-pass (Low Pass Filter (LPF)) band prominently showcases smooth variations across the graph, with connected regions exhibiting similar node colors. The high-pass (High Pass Filter (HPF)) band brings attention to deeper variations, emphasizing specific regions with distinct values from their connected regions. Meanwhile, the band-pass (BPF) band effectively highlights patches, aligning with the anticipated outcome.

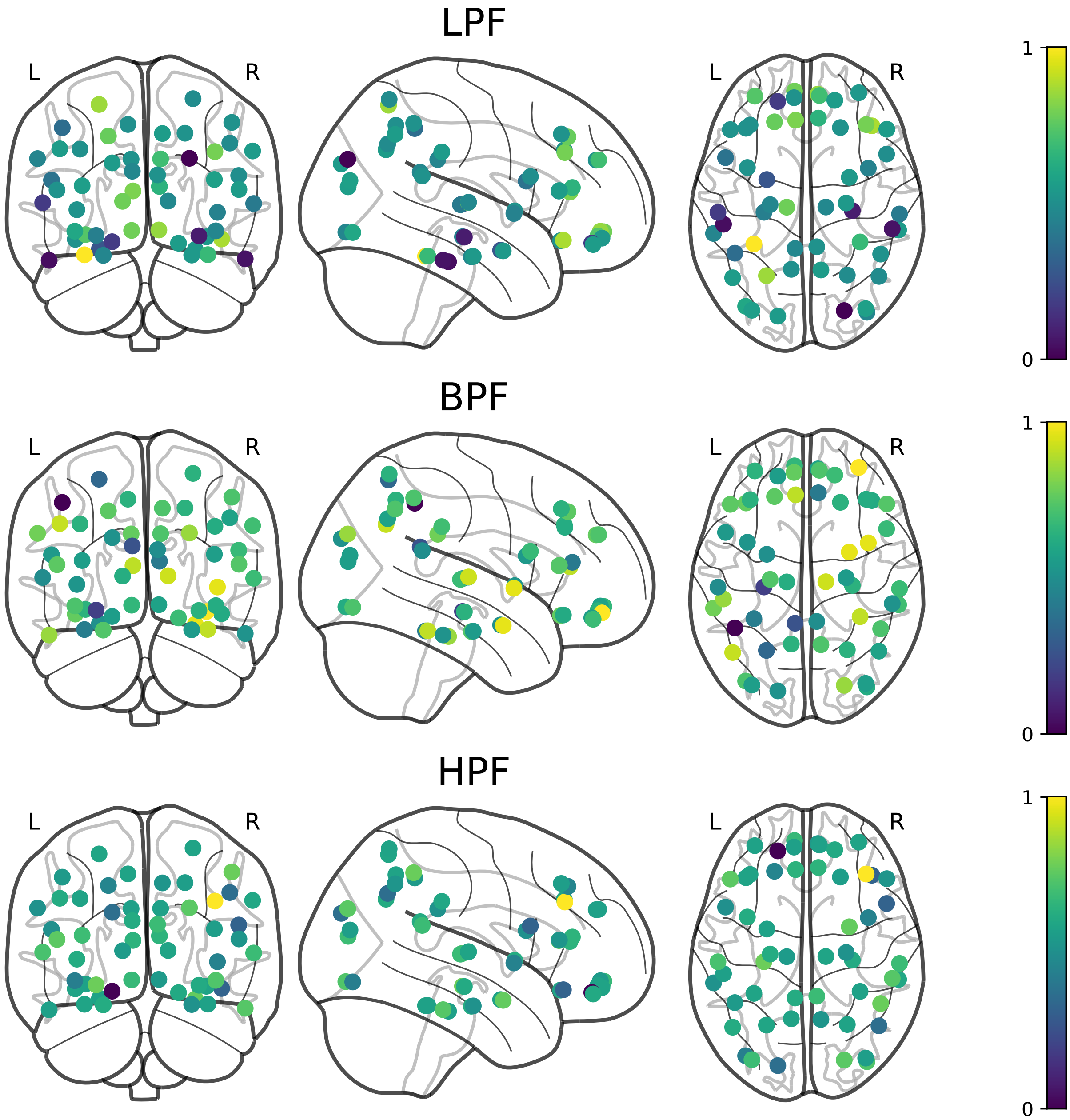

Figure 5.9 GFT of the graph signal at emotion HIGH time window, filtered into all 3 bands using sparsity-based approach averaged across all subjects, for M1

5.8 Claims and propositions

This study asks the question: given the complexity of empathy brain networks and the multi-modal stimulus used, can we build methods to model whole brain dynamics reflecting the behavioral responses to the narrative? By comparing the results obtained across different time intervals, particularly during the emotion HIGH duration and all-time average, several claims can be made.

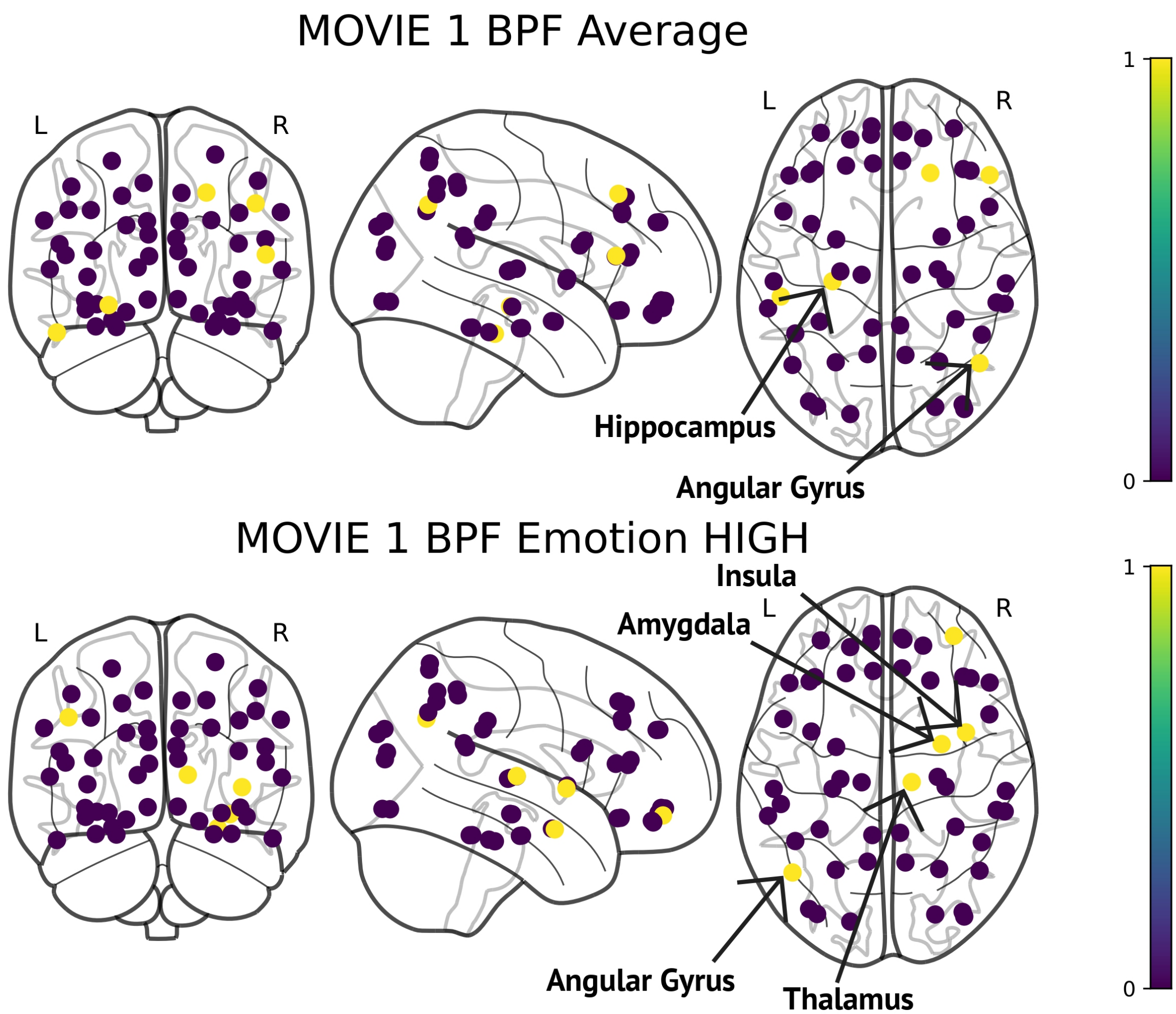

Figure 5.10 Region plot with the regions identified with with spectral filtering (BPF) using sparsity-based approach. The top 5 regions are highlighted. It shows variation in regions highlighted by averaging on all time (top) and during emotion HIGH (bottom) in M1

1. The sparsity-based method is able to model whole brain dynamics, reflecting behavioral responses to the stimulus, better than the other methods.

2. The pipeline proposed is able to perform denoising and capture connectivity dynamics related to a complex task like empathy.

3. The spectral-domain band-pass filtering is successful in highlighting a group of regions, related to empathy.

4. The sparsity-based method highlights robust connections between empathy supporting areas and contributes further knowledge to the field of empathy study.

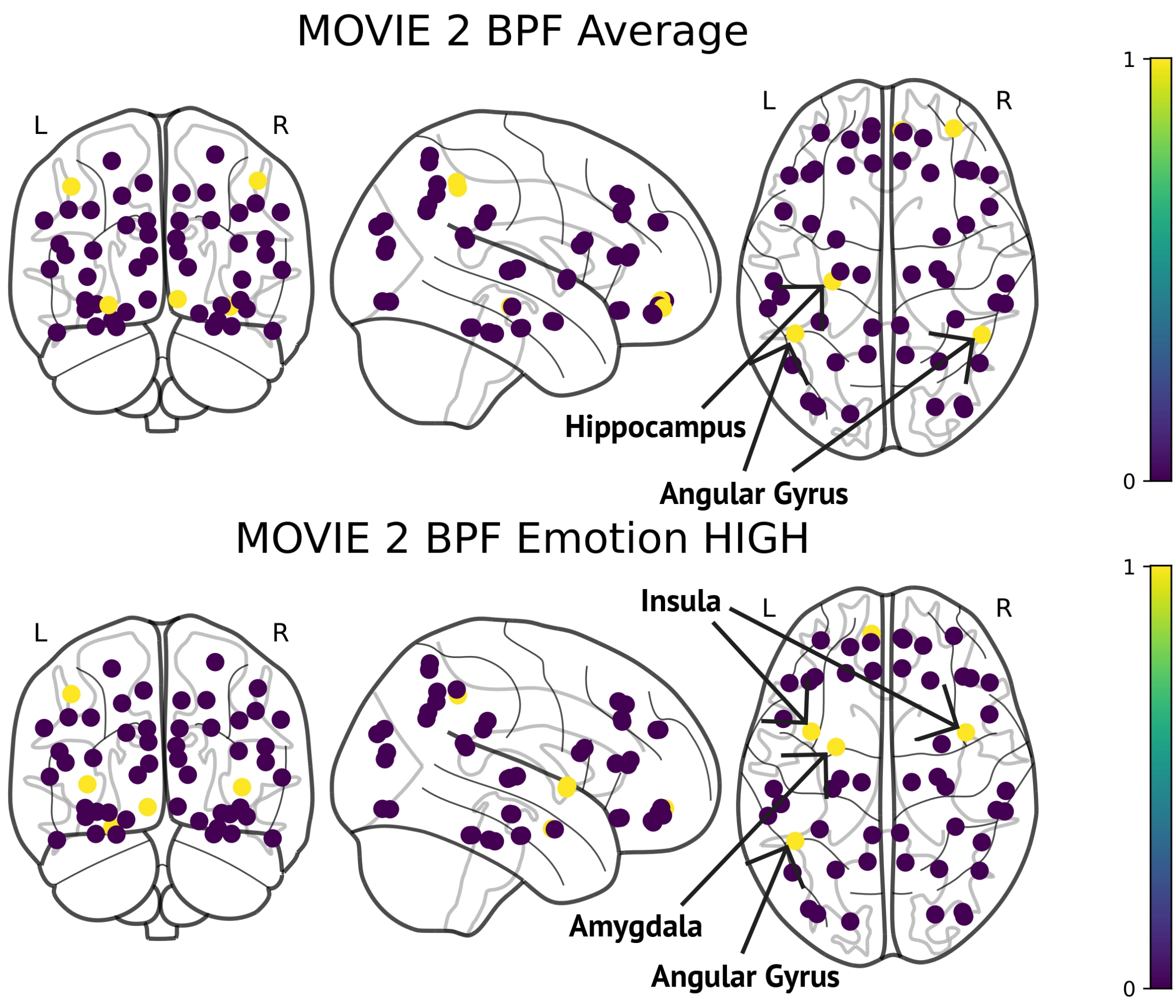

Figure 5.11 Region plot with the regions identified with with spectral filtering (BPF) using sparsity-based approach. The top 5 regions are highlighted. It shows variation in regions highlighted by averaging on all time (top) and during emotion HIGH (bottom) in M2

5.9 Discussion

Graph theory can prove to be useful in assessing brain network states, modeling inter-relationships between brain areas via edges and nodes using various metrics. This has been shown in previous studies to identify measures of neurological and psychiatric disorders [37, 38], emotional brain states, and task-aware effective brain connectivity [26]. However, it hasn't been utilized to study empathy-specific regions to the best of our knowledge. Here, we employed graph learning methods for whole-brain analysis to investigate brain activity in response to a naturalistic stimuli, expecting empathetic responses from participants.

Using GSP for fMRI empathy analysis offers several advantages. GSP captures complex brain network interactions, providing a deep understanding of functional connectivity and dynamics during empathetic processes. It can help uncover hidden patterns not easily discernible with traditional methods, potentially leading to novel insights. GSP's adaptability to individual differences accommodates inter-subject variability, allowing for both group and individual-level empathy-related brain activity analysis. It is important to note that in all the analyses, due to the absence of any ground truth for the functional connectivity networks, performance analysis has been done by comparing the emotion scale (behavioural) with secondary metrics extracted from the obtained networks, like graph cluster labels, edge-weight dynamics and region graph signal values in spectral filtering.

5.9.1 Comparison of different graph learning methods

The sparsity-based graph learning approach is well-suited for empathy-related tasks due to its capacity to efficiently capture selective and specific interactions among brain regions. This method adapts to individual differences, effectively representing dynamic and localized neural activations associated with empathy. The resulting sparse graphs enhance interpretability, reducing the susceptibility to noise, offering a focused and biologically plausible representation of the neural network. By suppressing non-specific connections, this approach enhances sensitivity to task-relevant signals, proving to be a powerful tool for investigating the neural correlates of empathy.

The sparsity-based approach consistently captures variations in the emotion scale (Figure 5.4), demonstrating an alignment of over 80% with the emotion contagion for all participants. When averaging subject responses, the distance, Pearson, smoothness, and sparsity-based methods exhibit 80%, 72%, 80%, and 88% match with the emotion scale, respectively. In comparison, Figure 5.5 demonstrates that the other approaches capture temporal variations to a lesser extent, achieving a low match with the emotion scale. This highlights the superiority of the sparsity-based approach to capture activations in a task-specific stimulus over existing methods, in both the movies.

In the observed graph clustering dynamics with the sparsity-based approach, a notable misalignment among clusters is observed before the 180 second mark, suggesting a lack of synchronization. However, post the initial period, a strong alignment is evident in both the movies, indicating a coherent configuration of clusters. The observed temporal shift in cluster alignment can be attributed to the gradual induction of empathy into the subjects rather than occurring suddenly, indicating a slow and steady build-up of empathetic responses. Notably, as empathy peaks in the subject, a synchronous alignment between the graph clusters and the emotion scale becomes evident in both the movies. This alignment provides compelling evidence that the obtained graph structures indeed correspond to an empathy network, further substantiating the temporal relationship between empathy induction and the configuration of functional brain networks.

Method	Avg. empathy score	Major regions
Distance [40]	82%	**Left Supramarginal Gyrus**, Right Superior Parietal, Right Superior Parietal, Left Inferior Occipital
Pearson's Correlation [9]	72%	Left Medial Orbital Frontal, **Right Fusiform Gyrus**, Left Inferior Occipital, Right Inferior Occipital
Smoothness [55]	82%	Right Middle Orbital Frontal, Right Angular Gyrus, Right Superior Parietal, Right Inferior Temporal
Sparsity	**88%**	**Right Amygdala**, **Right Insula**, **Right Thalamus**, Left Angular Gyrus, Right Middle Orbital Frontal

Table 5.2 Comparison of proposed pipeline of sparsity-based method with existing literature

Analyzing edge-weight variations between the Insula and Triangularis over time reveals that sparsity-based learning consistently detects activations more frequently than smoothness-based learning, particularly around the 200 second mark, where there is peak in the emotion scale. This indicates that smoothness-based learning may lead to fewer activations, especially in the Insula. As it tends to promote spatially smooth solutions, it may overlook localized variations in connectivity patterns related to task-specific activations. This constraint biases the learning process towards connections that exhibit gradual changes across the brain, potentially missing out on the fine-grained, task-specific connectivity dynamics that are crucial for understanding complex cognitive processes like empathy. Sparsity-based learning excels in identifying influential neighboring nodes, offering a more insightful perspective. Both methods exhibit peaks around 475 seconds, requiring further investigation for better interpretation, potentially linked to emotionally weighted movie scenes.

Pearson's correlation-based method produces noisy activations, hindering clear pattern understanding. This highlights the superior performance of the sparsity-based method in capturing relevant activations in empathy-related neural processes. In comparison with other methods concerning edge-weight activations and graph cluster alignment, the sparsity-based approach appears to outperform. Table 5.2 provides a tabulated summary of these results with existing methods.

5.9.2 Extraction of prominent regions and connections

In analysing edge-weight dynamics aligned with the emotion scale, key edges consistently activated during empathetic responses emerge as crucial markers, particularly in frontal and temporal regions, with notable emphasis on the Parahippocampal area for M1. Given the Parahippocampal region's well-established role in episodic memory and retrieval, its heightened activation aligns with the potential triggering of memory-based recall events during emotionally weighted movie scenes. This underscores the significance of the Parahippocampal edge in the interplay between empathetic responses and episodic memory retrieval.

The connectome-network analysis identifies the Insula, Amygdala, and Thalamus as central regions in empathy, aligning with established neuroscientific roles [60]. The Insula integrates emotional experiences, the Amygdala regulates emotions, and the Thalamus processes emotional cues. Lateral brain connections within the same bi-lateral regions suggest synchronized responses, facilitated by the corpus callosum. This inter-hemispheric coordination enhances the brain's processing of empathetic information. Averaging across all time reveals heightened activity in the ACC, Thalamus, and Precuneus. ACC's role in the DMN, Thalamus' sensory relay, and Precuneus' affective responses contribute to continuous engagement. During the emotion HIGH time window, Insula, Angular Gyrus, and frontal regions show prominent connections. As a part of our study, Angular Gyrus appears to get activated in correlation with the known emotion processing areas like the Amygdala in both the movies, highlighting its pivotal role in heightened empathy periods.

As a part of the spectral filtering-based analysis, Figure 5.9 displays patterns in low-pass (LPF), high-pass (HPF) and band-pass (BPF) bands, offering unique insights. LPF emphasizes brain regions associated with global network dynamics and slower oscillatory patterns, such as the DMN regions, while HPF highlights anomalies, proving ineffective in isolating empathy-specific networks as it consists of multiple regions with correlated activations. In the low-pass band, the lower graph frequencies, corresponding to smoother signals, tend to capture slow oscillations more prominently, as they exhibit coherent and consistent patterns of activity across the brain, making them more identifiable to spatial smoothing techniques. On the other hand, high-pass band focuses on regions that have activations that are not spatially smooth, leading to identifying outliers and anomalous regions in the brain. Notably, BPF strikes a balance between stability (almost constant throughout the regions) and anomaly (deeper localization), thereby isolating regions linked to emotional and empathetic processing during the emotion HIGH state.

Key regions, including Right Amygdala, Right Insula, Right Thalamus, Left Angular Gyrus, Right Middle Orbital Frontal, exhibit heightened activations in both the movies, emphasizing their role in immediate emotional responses. In the all-time-average analysis, sustained activations in Left Hippocampus, Right Angular Gyrus, Right Inferior Triangularis Frontal, Right Superior Frontal, Left Inferior Temporal suggest broader contributions to empathy across the entire stimulus duration. The activation in the Hippocampal area suggests memory retrieval taking place throughout the movie along with highlighting its contributions in emotion processing [61]. These findings align with literature [60–63], on neural correlates of empathy, reinforcing the selected BPF band as optimal for capturing empathy-related neural activity.

Both movies exhibited strong similarities across various analyses, ranging from similar patterns in graph cluster labels matching the emotion scale, to consistent highlighting of regions like Insula, Amygdala, and Angular in connectome-network and spectral filtering-based analyses. While the obtained regions are largely similar, potential differences in cognitive processing associated with each movie could contribute to subtle distinctions. However, regions highlighted in common can be claimed to have a stronger foundation in eliciting empathetic responses in the brain.

5.10 Conclusion

This chapter presents an application of the signal processing pipeline detailed in Chapter 4 to extract dynamic functional connectivity patterns between brain areas through the sparsity-based graph learning method. The sparsity-based approach consistently outperforms other methods in capturing variations in the emotion scale, aligning with over 80% match with the emotion scale across all participants. The temporal delay in alignment of graph cluster labels with the emotion scale indicates a gradual induction of empathy, supporting the method's effectiveness in capturing dynamic connectomes. Edge-weight dynamics analysis reveals the superiority of sparsity-based learning, particularly in detecting activations around the 200 second mark, emphasizing its ability to identify influential neighboring nodes.

A comprehensive method comparison highlights sparsity's ideal performance in emotion HIGH state, outperforming existing methods in terms of average empathy scores, edge-weight activations, and major regions involved. Connectome-network analysis underscores the pivotal role of the Insula, Amygdala, and Thalamus in empathy, with lateral brain connections facilitating synchronized responses. Spectral filtering analysis demonstrates the significance of the band-pass filter in isolating regions linked to emotional and empathetic processing during emotion HIGH states. The consistent activation of key regions like Amygdala, Insula, and Angular Gyrus further supports their critical role in immediate emotional responses. Overall, the obtained results across two movies reveal strong similarities in graph cluster labels, connectome-network analysis, and spectral filtering-based analyses, indicating robust neural correlates of empathy.

Chapter 6

Graph learning to compare task-based and resting state networks

6.1 Introduction

fMRI studies utilizing naturalistic stimuli, such as movies, offer a window into ecologically valid conditions, allowing for the examination of dynamic functional connectivity akin to resting-state conditions. In this comparative study, the analysis focuses on fMRI data collected from participants as they watched an 8 minute, 45 seconds full-length movie carefully selected to evoke empathy and elicit emotional responses within regions of the brain associated with empathy. This is compared with the resting state scenario, where the participants were instructed to rest and let the mind wander.

Resting-state captures brain function when subjects are not focused on a task and reveals brain networks involved in *top-down* processing. These networks mainly include the default mode network and dorsal attention network [33, 34], with minimal insights to the source of these triggers and hence termed 'mind-wandering'.

In contrast, task-fMRI engages focused brain functions like memory, emotions, language, decision-making, and sensory-differentiation, making it both *bottom-up* and *top-down* processing. Use of naturalistic stimuli (e.g. movies) as the task offers a more realistic setting, reflecting the complexity of real-life experiences. One such complex construct is empathy [13] which is the capacity to take others' perspectives and share their emotions or feelings. Empathy simultaneously involves *top-down* and *bottom-up* processing like mentalizing, or the cognitive evaluation of others' mental states, self-evaluation contexts, and emotional responses.

By discerning the intricate neural dynamics underlying empathy-related tasks and resting-state conditions, this study contributes to a deeper understanding of the networks involved in cognitive processes within real-life contexts. This exploration not only sheds light on the utility of resting-state fMRI for studying empathy but also enriches our comprehension of cognitive processes in naturalistic settings.

This study is based on the following hypothesis: The brain's dynamic response to natural stimuli, such as passive-viewing of movies, is considered "semi-controlled" by the context provided by the experimenter, compared to resting-state paradigms. Considering this distinction, comparing the functional connectivity between the two conditions will help differentiate the cognitive states and the inhibitory or antagonistic role of default-mode like networks in tasks.

The analysis was run on an NVIDIA RTX 3050Ti GPU using MATLAB and Python code. The codes used for this analysis are available online [64].

6.2 Summary of contributions and findings

The contributions and findings of this work are summarized here.

- Demonstration of the correlation between the time-varying graph-dissimilarity metric and the emotion scale (ground truth), indicating similarities and dissimilarities between task-based and resting-state networks during different emotional intervals.

- Further validation of findings through connectome-network analysis, revealing a significant overlap in highlighted edges during the emotion LOW interval in both task-based and resting-state networks.

- Highlighting specific connections, such as bilateral Superior Parietal connection (associated with visual tasks), identified only in the task-based network, indicative of the validity of networks obtained using the sparsity-based approach.

- Interpretation of reduced dissimilarity between task-based and resting-state networks during low-emotional intervals, suggesting stronger *top-down* processing akin to the resting-state, and increased dissimilarity during high-emotional intervals, indicative of directed brain responses to stimuli features.

- Confirmation of the hypothesis regarding variations in similarities between task-based and resting-state networks, emphasizing the superior performance of the sparsity-based method in identifying these variations.

6.3 Data and regions considered

This study utilized data from the movie (specifically, movie 1) as described in Section 5.2, along with resting-state data collected for a duration of 3 minutes as part of the same experiment. In this chapter, the term ‘task-based’ data will be used interchangeably with the movie data.

The selection of regions and resizing of masks followed a similar methodology outlined in Sections 5.3 and 5.4.

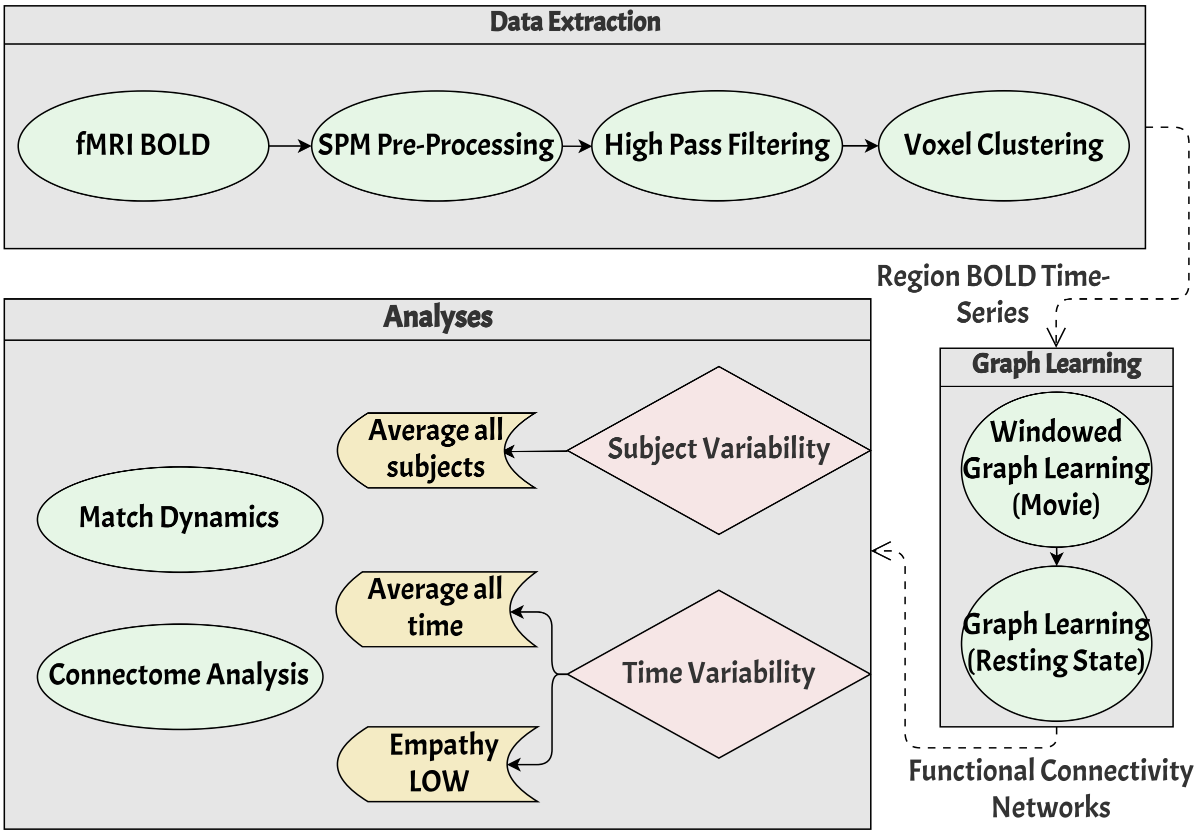

Figure 6.1 Pipeline used for fMRI BOLD signal functional connectivity comparison between resting state and task-based networks

6.4 Pipeline

The signal processing pipeline utilized in this study (shown in Figure 6.1) follows Chapter 4. The data extraction module, consistent with Chapter 4, includes pre-processing using SPM12, high-pass filtering, and voxel clustering. Subsequently, the resulting regional time-series are employed for functional connectivity analyses.

In the movie(task)-based analysis, graphs are constructed using a windowed approach with a duration of 16 seconds, allowing for temporal segmentation of the data. Conversely, a single graph is generated using the entire dataset without employing a windowed method for the resting-state analysis. The rationale behind learning a single graph for the resting state analysis is justified by the relative stationarity of a resting-state fMRI signal with respect to a task-specific fMRI signal. Throughout all the analyses, the same resting-state graph is utilized consistently across multiple time-varying movie-based graphs. This pipeline provides a comprehensive approach to analyzing fMRI data, offering valuable insights into the dynamics and interactions within brain networks.

6.5 Analyses

This section presents a comprehensive analysis focusing on two key dimensions: time and subjects. Temporal perspectives involve emphasizing time points with the lowest and highest emotional valence, labeled 'emotion LOW' (around 120-160 seconds interval) and 'emotion HIGH' (around 360-400 seconds interval), respectively, based on the emotion scale ratings as mentioned in Section 5.2. Subject-wise analyses involve averaging across all subjects. Both analyses are conducted separately for the movie and resting-state conditions, including match dynamics and connectome-network analyses.

6.5.1 Match Dynamics Analysis

Match dynamics analysis aims to quantify the similarity between the resting-state and movie-based networks at each time window. This similarity is measured by the number of common edges between the two networks. To calculate this, the adjacency matrices are thresholded to retain only the top 10 edges. The common edges are then identified by taking the element-wise product of the thresholded adjacency matrices. Summing this product over all rows and columns produces a scalar value, referred to as the graph-similarity metric, which quantifies the number of common edges.

The procedure is conducted over time to track the dynamics of the graph-similarity metric, which is then analyzed in relation to the emotion scale. To enhance interpretability, the negative of the obtained graph-similarity metric is used, defined as the graph-dissimilarity metric, quantifying the dissimilarity between the networks. Lower dissimilarity is anticipated during the emotion LOW interval and higher dissimilarity during the emotion HIGH interval, maintaining consistency with the hypothesis. The match between the time-varying graph-dissimilarity metric (averaged across subjects) and the emotion scale is quantified using the cross-correlation metric, assessing the similarity in shape between two signals. The analysis is limited to the top 10 edges to account for the sparsity of brain networks, focusing on impactful connections for improved interpretability.

6.5.2 Connectome-based Network Analysis

Connectome-network analysis employs edge thresholding on the obtained graphs, focusing on the top 5 connections. This highlights significant connections within the brain during distinct time intervals. The objective is to compare isolated connections in the emotion LOW interval between the movie and resting-state, providing insights into connectivity patterns and identifying regions characterized by robust connections. Consistent with the hypothesis suggesting similarities in mind-wandering during resting-state and low-emotion intervals in a movie, a comparison is undertaken across all four graph learning methods in the pipeline, focusing on connectivity in resting-state in contrast to the emotion LOW interval.

6.6 Results

6.6.1 Task-based (MOVIE)

6.6.1.1 Emotion LOW interval

In the movie-based analysis, connections involving bilateral Superior Parietal regions are exclusively observed, likely attributed to visual processing responses stimulated by the movie. Further, regions like the Left Middle Orbital Frontal ↔ Left Middle Frontal, Left Thalamus ↔ Right Thalamus, and Right Amygdala ↔ Left Angular Gyrus are also identified in the movie-based network during the interval with low emotional valence.

6.6.1.2 All-time average

When averaged across all time, the movie-based network exhibits distinct connections in regions associated with empathy, such as the Amygdala, ACC, and Precuneus, reflecting activations specific to empathy-related stimuli

6.6.2 Resting state

As mentioned in Section 6.4, only one functional network is generated for the resting-state analysis. Connections involving the bilateral Anterior Cingulate Cortex (PCC) are uniquely present in the resting-state network, underscoring the role of the PCC as a crucial component of the DMN specific to resting-state conditions. Other connections include Left Middle Orbital Frontal ↔ Left Middle Frontal, Left Thalamus ↔ Right Thalamus, and Right Amygdala ↔ Left Angular Gyrus, which are in common with the ones obtained during the emotion LOW interval in the movie-based analysis.

6.6.3 Comparison

6.6.3.1 Match dynamics analysis

In Figure 6.2 (top), the contrast between the time-varying graph-dissimilarity metric and the emotion scale rating, utilizing the sparsity-based method, is depicted. Both the signals plotted are mean shifted and variance normalized to 1 for visualization. It is important to note that the graph-dissimilarity metric serves as a quantification of connection-based dissimilarity between the resting-state and movie-based networks. In essence, lower values of this metric signify a higher similarity between the networks, whereas higher values indicate greater dissimilarity.

Observing the alignment between the graph-dissimilarity metric and the emotional scale, notable patterns emerge. In the emotion LOW interval (shaded green), wherein the emotion scale has a dip, a corresponding decrease in the graph-dissimilarity metric is noted, although with a slight temporal delay. This observation implies the presence of common edges between the movie and resting-state networks

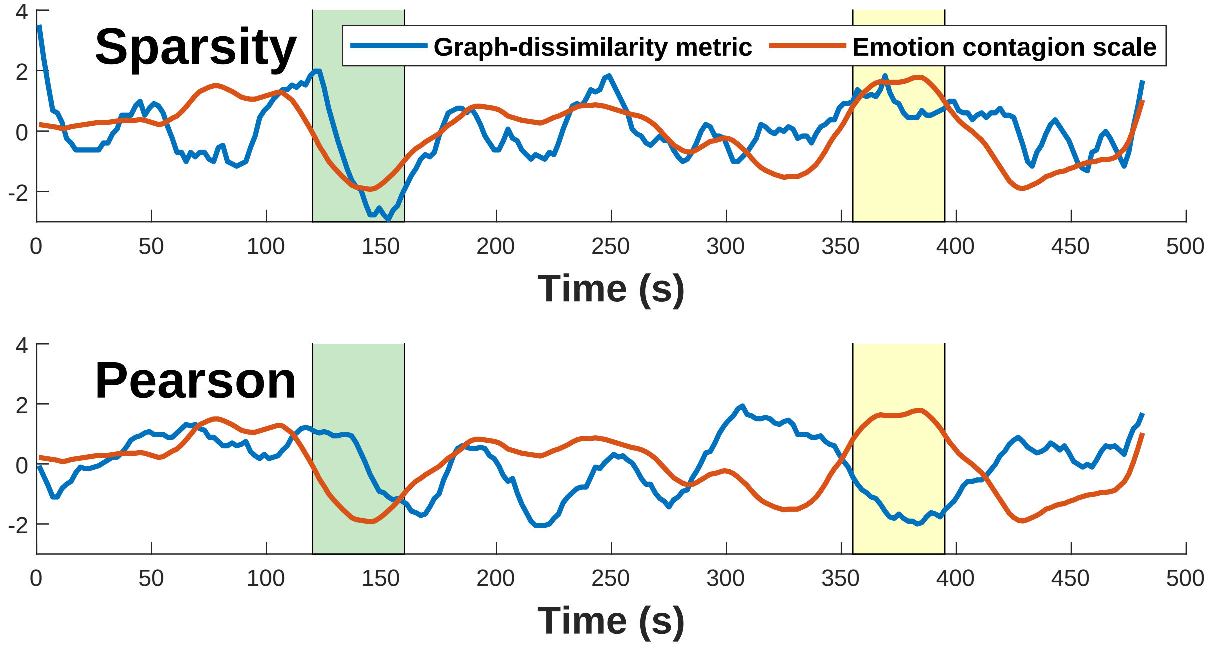

Figure 6.2 Match dynamics: Comparison between the time-varying graph dissimilarity metric and the emotion contagion scale using the sparsity-based (top) and Pearson's correlation-based (bottom) method. The blue curve denotes the dissimilarity metric analogous to the number of different connections between the movie-based and resting-state networks. Both the curves are mean shifted and variance normalized to 1 for visualization.

during periods of reduced emotional intensity, supporting the notion of shared connectivity patterns during states akin to mind-wandering and the resting-state.

Conversely, during the emotion HIGH interval (shaded yellow), characterized by an upsurge in the emotion scale, a corresponding spike in the graph-dissimilarity metric is observed. This phenomenon suggests a reduction in the number of common edges between the movie and resting-state networks during intervals of heightened emotional intensity. Such findings substantiate the hypothesized similarity between states of mind-wandering observed during periods of low emotional arousal and the resting-state, further enriching our understanding of brain dynamics during various emotional states.

In contrast to the sparsity-based method, Figure 6.2 (bottom) presents a comparison of the time-varying graph-dissimilarity metric with the emotion scale utilizing the Pearson's correlation-based method. Unlike the consistent alignment observed with the sparsity-based approach, analysis reveals that the graph-dissimilarity metric derived from the Pearson's correlation-based method does not consistently align with the emotional scale across various time intervals, emphasizing its limitations in accurately capturing the relationship between movie-induced and resting-state networks.

Notably, unexpected observations arise, particularly during the empathy HIGH time-window. Here, a dip in the distance metric implies a high degree of similarity between the two networks. This unex-

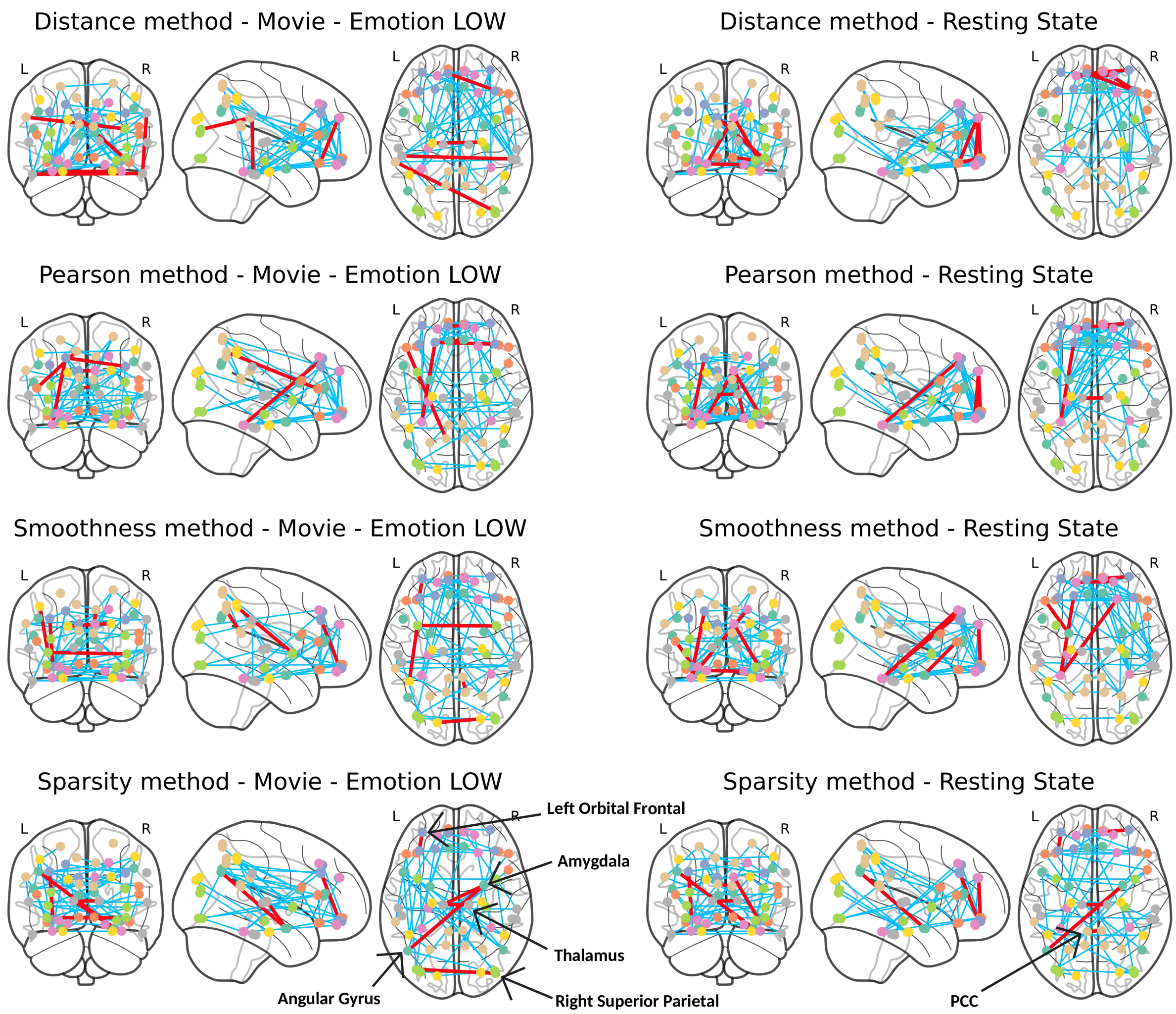

Figure 6.3 Comparison of top-5 connections, across all methods in the emotion LOW interval, contrasted between movie (task) and resting-state. The red connections denote the strongest 5 connections in the network.

pected finding suggests the potential presence of the resting-state network during periods of heightened empathy, contradicting previous observations documented in Chapter 5.

Comparison with other methods highlights the performance differences, showcasing averaged cross-correlation percentages of 81% for the distance-based method, 84% for Pearson's correlation-based method, 90% for the smoothness-based method, and notably, 98% for the sparsity-based method. These findings reinforce the conclusions drawn in the previous work in Chapter 5, underscoring the superior performance of the sparsity-based method in effectively capturing the intricate relationship between movie-induced and resting-state networks.

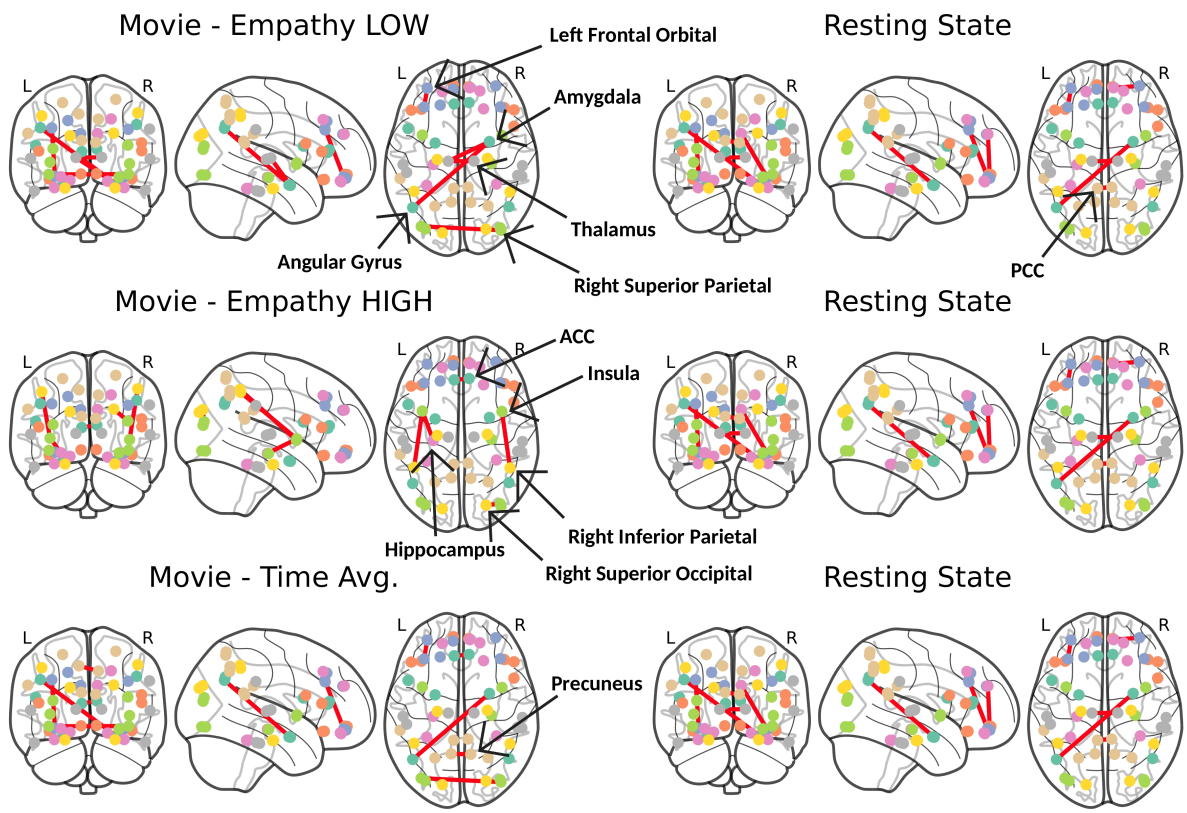

Figure 6.4 Comparison of top-5 connections, across time - emotion LOW interval (top), emotion HIGH interval (middle) and all-time average (bottom) in the movie (left), contrasted against resting-state (right) using the sparsity-based method. The red connections denote the strongest 5 connections in the network.

6.6.3.2 Connectome-based network analysis

The results obtained from the connectome-network analysis show similarities in the edges highlighted during the emotion LOW interval between the movie-based and resting-state networks using the sparsity-based graph learning method. Figure 6.3 illustrates this comparison across all methods, shedding light on the connections observed during the emotion LOW interval in both movie-based and resting-state conditions.

Several connections emerge consistently across both movie-based and resting-state networks during the emotion LOW interval. Connections such as Left Middle Orbital Frontal $\leftrightarrow$ Left Middle Frontal, Left Thalamus $\leftrightarrow$ Right Thalamus, and Right Amygdala $\leftrightarrow$ Left Angular Gyrus are consistently identified in common, indicating shared network activations during periods of low emotional valence.

Nevertheless, the connectome-network analysis reveals intriguing distinctions between the movie-based and resting-state networks. For instance, connections involving bilateral Superior Parietal regions are exclusive to the movie-based network, likely attributed to visual processing responses stimulated by the movie. Conversely, connections involving the bilateral PCC are uniquely present in the resting-state network, underscoring the role of the PCC as a crucial component of the DMN specific to resting-state conditions.

These findings underscore the efficacy of the sparsity-based approach in accurately identifying network activations consistent with the presented stimulus. Moreover, the sparsity-based method effectively captures shared connections between movie-based and resting-state networks during empathy-LOW and resting-state tasks, validating the initial hypothesis. In comparison, alternative methods such as distance-based, Pearson's correlation-based, and smoothness-based approaches fail to isolate common connections between the networks during the empathy LOW time-window and resting-state conditions.

Furthermore, Figure 6.4 provides a comprehensive overview of the extracted connections in the all-time-average comparison between movie and resting-state networks. Notably, the movie-based network exhibits distinct connections in regions associated with empathy, such as the Amygdala, ACC, and Precuneus, reflecting activations specific to empathy-related stimuli. Conversely, the resting-state network displays a different set of highlighted edges, emphasizing connections unique to the resting-state condition. This analysis reaffirms the distinct network dynamics observed during empathy HIGH intervals, as observed in the previous study in Chapter 5.

6.7 Claims and propositions

This study is based on the hypothesis: The brain's dynamic response to natural stimuli, such as passive-viewing of movies, is considered "semi-controlled" by the context provided by the experimenter, compared to resting-state paradigms. By comparing the results obtained across different time intervals, particularly during the emotion LOW and HIGH durations, several claims can be made.

1. The hypothesis is supported with the match dynamics analysis and verified in detail with the intricate connections in common between the movie-based and resting-state networks, as a part of the connectome-based network analysis.

2. The sparsity-based method effectively captures both similarities and variations between the movie-based and resting-state networks, aligning with the hypothesis.

6.8 Discussion

Graph theory, a robust tool for assessing brain network states, has been extensively applied in studies on various brain conditions and in studies looking at emotional responses [26, 37, 38]. While previous research explored graph learning methods for empathy-specific conclusions in Chapter 5, this study focuses on comparing responses to resting-state and an emotion-inducing naturalistic stimuli (movie).

GSP proves valuable, offering deep insights into functional connectivity during task-based (empathetic) processes and resting-state, adaptable to individual differences. The work hypothesized that tasks with both *top-down* and *bottom-up* processing as afforded in a directed or controlled narrative could share connectivity similarities with resting-state (*top-down*) neural activity, while also showing distinct activation. Our analyses aim to reveal distinctions and parallels between passive-viewing of a movie and resting-state connectivity patterns, considering the emotional valence scales reported.

The findings demonstrate the correlation between the time-varying graph-dissimilarity metric and the emotion scale. Throughout the discussion, we refer to the movie-based network as $\mathbf{X}$ and the resting-state network as $\mathbf{Y}$. The graph-dissimilarity metric, representing the connection-based dissimilarity between $\mathbf{X}$ and $\mathbf{Y}$, aligns notably with the emotion scale, particularly in the emotion LOW and HIGH intervals, indicating similarities between $\mathbf{X}$ and $\mathbf{Y}$ during emotion LOW states, and dissimilarities during emotion HIGH states using the sparsity-based method (Figure 6.2 (top)). The observed alignment of activation with a slight lag could have multiple reasons like the windowed nature of the graph learning process or due to the inherent hemodynamic response lag in BOLD fMRI signals. This lag results in the activation appearing in the scanned signal approximately 5-7 seconds after the actual stimulus duration. This temporal delay is evident in Figure 6.2 (top), particularly in the emotion LOW interval. Currently, the underlying reason for the lag requires further studies to eliminate scanning-machine effects by using a time-locked trigger to match the events in the movie to the hemodynamic response.

Furthermore, the connectome-network analysis indicates a significant overlap in highlighted edges during the emotion LOW interval in $\mathbf{X}$ and $\mathbf{Y}$. Notably, $\mathbf{X}$ highlights bilateral Superior Parietal connection absent in $\mathbf{Y}$, a network attributed to visual processing. Interestingly, the shared connections and the bilateral Superior Parietal connection are highlighted in the sparsity-based method alone, indicative of the validity of the networks obtained using the sparsity-based approach on both task-based and resting-state. Figure 6.4 demonstrates the contrast in extracted connections during emotion LOW, HIGH, and all-time-average analyses. Notably, the emotion HIGH time window reveals diverse highlighted edges in the resting-state network compared to the movie-based network. Empathy-specific regions exhibit highlighted connections, contributing to the 'empathy network' identified in the previous work in Chapter 5. The all-time-average analysis shows contributions from both networks, alongside Left Precuneus and Right Precuneus. This confirms the validity of the sparsity-based method in differentiating between networks during low and high emotional cues.

After examining the findings in relation to our hypothesis, the reduced dissimilarity in $\mathbf{X}$ and $\mathbf{Y}$ during low-emotional intervals suggests that: although the movie acts as a stimulus, it is possible the activation or processing during this interval might not be potent enough to generate significant stimulus-specific brain responses. This results in activity comparable to the resting-state, which indicates stronger *top-down* processing, not specific to the stimuli features. On the contrary, increased dissimilarity during high-emotional intervals implies that: the movie provides a strong stimulus to the brain during this interval and directs its response to follow the same signature as the stimuli features, thus distinguishing itself from an uncontrolled response in the resting-state. This confirms the hypothesis presented, with specific emphasis on the sparsity-based method, proving to outperform others in identifying variations in similarities between the movie-based and resting-state networks, in agreement with the conclusions drawn in the previous work in Chapter 5.

6.9 Conclusion

This study explores the hypothesis that brain responses to natural stimuli, such as watching movies, exhibit controlled behavior during high emotional scenarios and resemble resting-state activity during low emotional cues. Our analysis confirms this hypothesis, revealing distinct connectivity patterns during high and low emotional cues. Using a sparsity-based method, we achieve 98% match with emotion ratings, whereas Pearson's correlation-based method achieves 84% match. However, challenges in graph learning arise with longer narratives due to the high computational complexity. Future work could integrate structural connectivity information to enhance functional connectivity analysis, ensuring networks consider temporal similarities and anatomical priors for robustness.

Chapter 7

Conclusion

This thesis presents an fMRI signal processing pipeline utilizing the optimization based graph learning methods to extract dynamic functional connectivity patterns between brain areas. In an exploratory analysis to identify the best performing graph learning method in identifying empathy networks during a naturalistic stimuli, the results consistently demonstrate the superiority of the sparsity-based approach in capturing variations in the emotion contagion scale, achieving over 80% accuracy across all participants. The observed temporal alignment in graph cluster labels with the emotion scale supports the method's efficacy in capturing dynamic connectomes, while edge-weight dynamics analysis highlights its ability to detect activations around specific time intervals in the movie rated to possess a high emotional valence.

A method comparison underscores the ideal performance of sparsity-based learning in emotion HIGH states, outperforming existing methods in terms of average empathy scores, edge-weight activations, and major regions involved. Connectome-network analysis reveals the pivotal role of regions like the Insula, Amygdala, and Thalamus in empathy, with lateral brain connections facilitating synchronized responses. Furthermore, spectral filtering analysis emphasizes the significance of the spectral band-pass filter in isolating regions linked to emotional and empathetic processing during emotion HIGH states.

Further, in a comparative analysis between task-based and resting-state connectivity patterns, this thesis explores the hypothesis that brain responses to naturalistic stimuli, such as watching movies, exhibit controlled behavior during high emotional scenarios and resemble resting-state activity during low emotional intervals. The analysis confirms this hypothesis, revealing distinct connectivity patterns during high and low emotional cues. Using a sparsity-based method, we achieve 98% match with emotion ratings, whereas Pearson's correlation-based method achieves 84% match.

In conclusion, by leveraging the sparsity-based method, the study reveals to achieve a high match with emotion ratings, suggesting its potential for robust functional connectivity analysis in the context of complex constructs like empathy.

However, this thesis also highlights limitations associated with using GSP for fMRI empathy analysis, including variability in graph construction with the solver used and computational intensity.

For future investigations, this thesis suggests exploring graph wavelet transform-based analyses to conduct a more in-depth examination of spectral bands, thereby providing deeper localization within the brain. Additionally, a comparative analysis involving a condensed version of the movie, and a structural connectivity network could offer insights into the dynamics of brain activity across different conditions. Another promising research direction would be to incorporate prior information from structural connectivity into the learning process for functional connectivity, which could open new possibilities for a better understanding of neural interactions. Integrating structural connectivity information into functional connectivity analysis could enhance network robustness by considering both temporal similarities and anatomical priors.

Addressing these limitations and exploring future directions could further enhance the understanding of neural interactions and their implications for empathy processing.

Appendix A

Plot for the movies

A.1 M1 - ”These Times”

The film is directed by Ramy El Gabry, starring Khaled Megald, Abdallah Alnahas and Awatef Helmy and is set in Cairo, Egypt. The short 11 minute movie, opens with a scene that shows a young man dressed for office standing in his balcony and sees an old woman being led by a man to a seat facing the water body in front of his house. The woman is instructed by her son to wait for him, as he has to go for some work. He gives her a piece of paper saying it has his contact details. The woman is shown sitting on the seat, watching people go by and also talks to a young child who halts at the seat. The man who sees her in the morning, returns from office in the evening and see her still sitting at the same place. He crosses the road and walks over to her. He starts a conversation, and she mentions that she is waiting for her son to return. She also narrates how she will be seeing her grandson for the first time, as she stays in the village, and shows the man the chain she bought for her grandson and a photograph. Being thirsty she accepts water from the man. He then offers to call her son, to find out the reason for the delay. Initially she hesitates as she does not want to trouble the son and the man too. But then relents and hands over the slip of paper. The man opens the paper and sees that the message written by the son is “whoever finds this woman, please move her to an old age home”. The last scene zooms in as the man’s expressions is understood by the woman and her face reflects acute sorrow.

The link for the movie is also provided [65].

A.2 M2 - “Most “(re-titled “The Bridge”)

directed by Bobby Garabedian , written and produced by William Zabka had won the 2003 Palm springs – best of festival-award and other nominations too. The film is about a father employed as the railroad drawbridge operator, who takes his eight-year old son to work one-day. They both walk to the engine room, and the father tells his son to stay at the edge of a nearby lake and try fishing. A ship comes by and the bridge is drawn up. The bridge has a train track and has to be locked down for the train. On that day, the train happens to arrive early and the son notices the smoke from the engine and shouts a warning to his father. But the father does not hear it over the noise in the engine room. The son, runs towards the manual lever at the junction where the bridge rises up. The father looks out of the window and sees that his son is not near the lake, he then notices the train and realizes that his son is trying to close the lever. Meanwhile the boy, when attempting to move the lever, slips and falls on the gears. The father has to make the cruel decision whether to pull the lever down and save the lives of hundreds in the train or his son who will be crushed to death if the lever is pulled down. With great agony, he pulls the lever down and the train chugs by, while he rushed down the engine room a women passenger looks out of the window of the train to see the father crying in anguish, oblivious of the sacrifice of the father has made. The movie ends, with the father in a new city and seeing the same woman cross the road with a little boy, and realizes that life should go on.

The 29 minute original length was edited to fit in the narrative which features the son and father while editing out the narrative of the people in the train. The short emotional scenes selected for the experiment were 14-20 seconds of the part when the father is seen crying in anguish – depiction of high emotions and the neutral clipping was of the father and son walking towards the engine room.

The link for the movie is also provided [66].

Appendix B

Emotion contagion scale

The emotion scale for M1 is shown in Figure B.1, and for M2 is shown in Figure B.2.

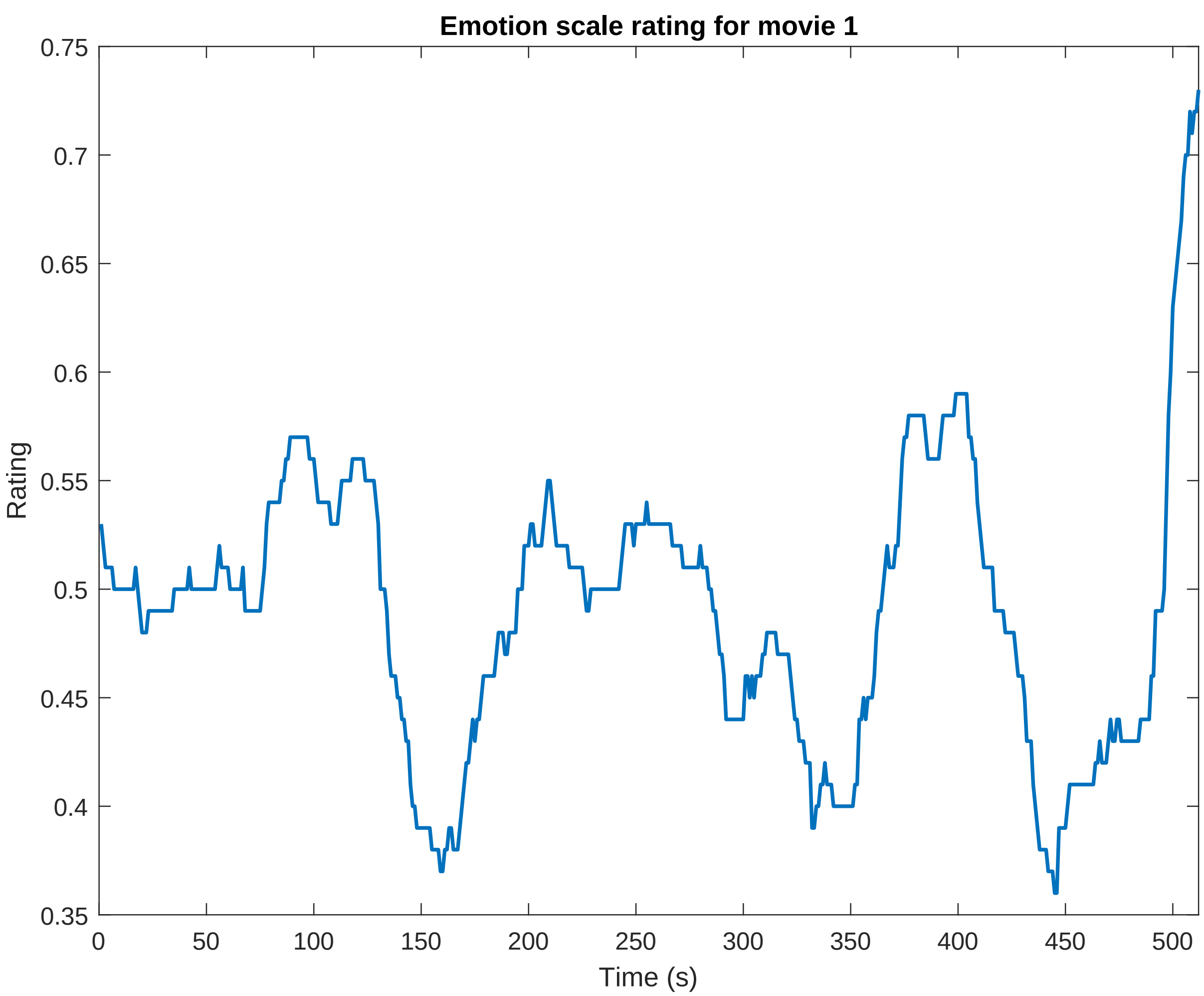

Figure B.1 Emotion scale plot for M1

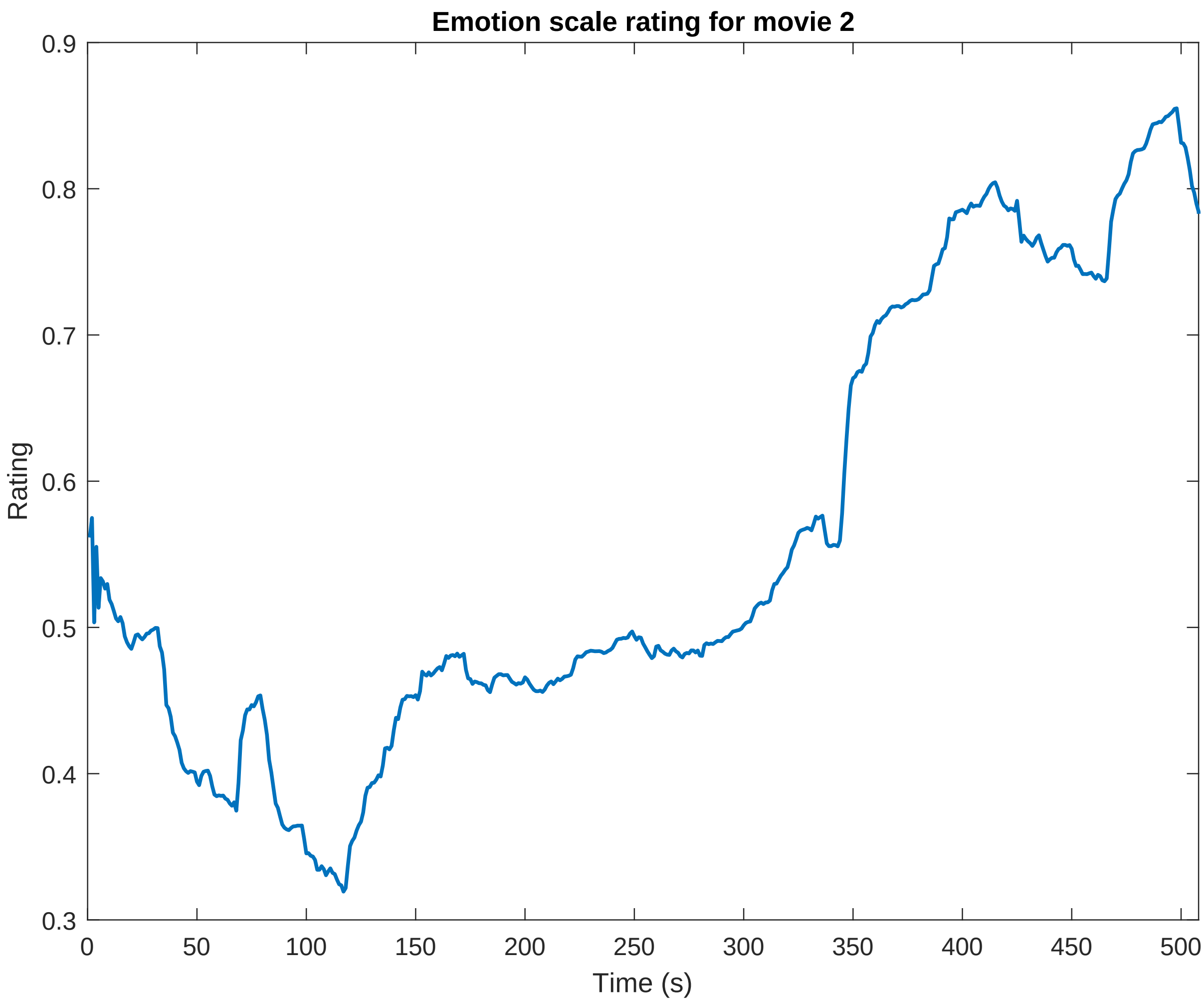

Figure B.2 Emotion scale plot for M2

Appendix C

List of regions

Table C.1 and Table C.2 list all the 54 bilateral regions considered for the study along with their corresponding AAL region number.

Number	Name	Number	Name	Number	Name
2101	Left Superior Frontal	3001	Left Insula	5401	Left Fusiform Gyrus
2102	Right Superior Frontal	3002	Right Insula	5402	Right Fusiform Gyrus
2111	Left Orbital Superior Frontal	4001	Left ACC	6101	Left Superior Parietal
2112	Right Orbital Superior Frontal	4002	Right ACC	6102	Right Superior Parietal
2201	Left Middle Frontal	4021	Left PCC	6201	Left Inferior Parietal
2202	Right Middle Frontal	4022	Right PCC	6202	Right Inferior Parietal
2211	Left Orbital Middle Frontal	4101	Left Hippocampus	6211	Left Supramarginal Gyrus
2212	Right Orbital Middle Frontal	4102	Right Hippocampus	6212	Right Supramarginal Gyrus
2301	Left Inferior Opercularis Frontal	4111	Left Parahippocampus	6221	Left Angular Gyrus

Table C.1 List of brain regions and their corresponding AAL Atlas region number

Number	Name	Number	Name	Number	Name
2302	Right Inferior Opercularis Frontal	4112	Right Parahippocampus	6222	Right Angular Gyrus
2311	Left Inferior Triangularis Frontal	4201	Left Amygdala	6301	Left Precuneus
2312	Right Inferior Triangularis Frontal	4202	Right Amygdala	6302	Right Precuneus
2321	Left Inferior Orbital Frontal	5101	Left Superior Occipital	7101	Left Thalamus
2322	Right Inferior Orbital Frontal	5102	Right Superior Occipital	7102	Right Thalamus
2601	Left Superior Medial Frontal	5201	Left Middle Occipital	8111	Left Superior Temporal
2602	Right Superior Medial Frontal	5202	Right Middle Occipital	8112	Right Superior Temporal
2611	Left Orbital Medial Frontal	5301	Left Inferior Occipital	8301	Left Inferior Temporal
2612	Right Orbital Medial Frontal	5302	Right Inferior Occipital	8302	Right Inferior Temporal

Table C.2 List of brain regions and their corresponding AAL Atlas region number

Bibliography

[1] S. Baron-Cohen and S. Wheelwright, "The empathy quotient: an investigation of adults with asperger syndrome or high functioning autism, and normal sex differences," *Journal of autism and developmental disorders*, vol. 34, pp. 163–175, 2004.

[2] P. L. Lockwood, C. L. Sebastian, E. J. McCrory, Z. H. Hyde, X. Gu, S. A. De Brito, and E. Viding, "Association of callous traits with reduced neural response to others' pain in children with conduct problems," *Current Biology*, vol. 23, no. 10, pp. 901–905, 2013.

[3] A. Ortega, P. Frossard, J. Kovačević, J. M. F. Moura, and P. Vandergheynst, "Graph signal processing: Overview, challenges, and applications," *Proceedings of the IEEE*, vol. 106, no. 5, pp. 808–828, 2018.

[4] M. E. Raichle, "The brain's default mode network," *Annual review of neuroscience*, vol. 38, pp. 433–447, 2015.

[5] M. D. Greicius, K. Supekar, V. Menon, and R. F. Dougherty, "Resting-state functional connectivity reflects structural connectivity in the default mode network," *Cerebral cortex*, vol. 19, no. 1, pp. 72–78, 2009.

[6] S. B. Eickhoff, S. Jbabdi, S. Caspers, A. R. Laird, P. T. Fox, K. Zilles, and T. E. Behrens, "Anatomical and functional connectivity of cytoarchitectonic areas within the human parietal operculum," *Journal of Neuroscience*, vol. 30, no. 18, pp. 6409–6421, 2010.

[7] L. K. Paul, "Developmental malformation of the corpus callosum: a review of typical callosal development and examples of developmental disorders with callosal involvement," *Journal of neurodevelopmental disorders*, vol. 3, pp. 3–27, 2011.

[8] L. Stanković, M. Daković, and E. Sejdić, *Introduction to Graph Signal Processing*. Cham: Springer International Publishing, 2019, pp. 3–108.

[9] M. Rubinov and O. Sporns, "Complex network measures of brain connectivity: Uses and interpretations," *NeuroImage*, vol. 52, no. 3, pp. 1059–1069, 2010, computational Models of the Brain. [Online]. Available: https://www.sciencedirect.com/science/article/pii/S105381190901074X

[10] U. Hasson, Y. Nir, I. Levy, G. Fuhrmann, and R. Malach, "Intersubject synchronization of cortical activity during natural vision," *Science (New York, N.Y.)*, vol. 303, pp. 1634–40, 04 2004.

[11] K. Vemuri and B. Surampudi, "Evidence of stimulus correlated empathy modes – group ica of fmri data," *Brain and cognition*, vol. 94C, pp. 32–43, 01 2015.

[12] P. Tikka, A. Väljamäe, A. de Borst, R. Pugliese, N. Ravaja, M. Kaipainen, and T. Takala, "Enactive cinema paves way for understanding complex real-time social interaction in neuroimaging experiments," *Frontiers in Human Neuroscience*, vol. 6, 2012. [Online]. Available: https://www.frontiersin.org/articles/10.3389/fnhum.2012.00298

[13] M. Melloni, V. Lopez, and A. Ibanez, "Empathy and contextual social cognition," *Cognitive, Affective, & Behavioral Neuroscience*, vol. 14, no. 1, pp. 407–425, Mar 2014.

[14] E. Simony, C. J. Honey, J. Chen, O. Lositsky, Y. Yeshurun, A. Wiesel, and U. Hasson, "Dynamic reconfiguration of the default mode network during narrative comprehension," *Nature Communications*, vol. 7, no. 1, p. 12141, Jul 2016. [Online]. Available: https://doi.org/10.1038/ncomms12141

[15] J. Decety, C. Chen, C. Harenski, and K. Kiehl, "An fmri study of affective perspective taking in individuals with psychopathy: imagining another in pain does not evoke empathy," *Frontiers in Human Neuroscience*, vol. 7, 2013. [Online]. Available: https://www.frontiersin.org/articles/10.3389/fnhum.2013.00489

[16] J. N. Beadle and C. E. de la Vega, "Impact of aging on empathy: Review of psychological and neural mechanisms," *Frontiers in Psychiatry*, vol. 10, 2019. [Online]. Available: https://www.frontiersin.org/articles/10.3389/fpsyt.2019.00331

[17] Y. Akitsuki and J. Decety, "Social context and perceived agency affects empathy for pain: An event-related fmri investigation," *NeuroImage*, vol. 47, no. 2, pp. 722–734, 2009. [Online]. Available: https://www.sciencedirect.com/science/article/pii/S1053811909004789

[18] T. Singer, B. Seymour, J. O'Doherty, H. Kaube, R. J. Dolan, and C. D. Frith, "Empathy for pain involves the affective but not sensory components of pain," *Science*, vol. 303, no. 5661, pp. 1157–1162, 2004. [Online]. Available: https://www.science.org/doi/abs/10.1126/science.1093535

[19] J. Decety and Y. Moriguchi, "The empathic brain and its dysfunction in psychiatric populations: implications for intervention across different clinical conditions," *BioPsychoSocial Medicine*, vol. 1, no. 1, p. 22, Nov 2007. [Online]. Available: https://doi.org/10.1186/1751-0759-1-22

[20] Y. Cheng, C.-Y. Yang, C.-P. Lin, P.-L. Lee, and J. Decety, "The perception of pain in others suppresses somatosensory oscillations: A magnetoencephalography study," *NeuroImage*, vol. 40, no. 4, pp. 1833–1840, 2008. [Online]. Available: https://www.sciencedirect.com/science/article/pii/S1053811908001146

[21] P. Ruby and J. Decety, "How Would You Feel versus How Do You Think She Would Feel? A Neuroimaging Study of Perspective-Taking with Social Emotions," *Journal of Cognitive Neuroscience*, vol. 16, no. 6, pp. 988–999, 07 2004. [Online]. Available: https://doi.org/10.1162/0898929041502661

[22] D. Tomlin, A. Nedic, D. Prentice, P. Holmes, and J. Cohen, "The neural substrates of social influence on decision making," *PloS one*, vol. 8, p. e52630, 01 2013.

[23] K. Vemuri and B. Surampudi, "An exploratory investigation of functional network connectivity of empathy and default mode networks in a free-viewing task," *Brain connectivity*, vol. 5, 04 2015.

[24] J. Zaki, T. D. Wager, T. Singer, C. Keysers, and V. Gazzola, "The anatomy of suffering: Understanding the relationship between nociceptive and empathic pain," *Trends in Cognitive Sciences*, vol. 20, no. 4, pp. 249–259, 2016. [Online]. Available: https://www.sciencedirect.com/science/article/pii/S1364661316000449

[25] J.-P. Kauppi, I. Jääskeläinen, M. Sams, and J. Tohka, "Inter-subject correlation of brain hemodynamic responses during watching a movie: localization in space and frequency," *Frontiers in Neuroinformatics*, vol. 4, 2010. [Online]. Available: https://www.frontiersin.org/articles/10.3389/fninf.2010.00005

[26] Y. Yu, X. Kan, H. Cui, R. Xu, Y. Zheng, X. Song, Y. Zhu, K. Zhang, R. Nabi, Y. Guo, C. Zhang, and C. Yang, "Learning task-aware effective brain connectivity for fMRI analysis with graph neural networks (extended abstract)," in *2022 IEEE International Conference on Big Data (Big Data)*, 2022, pp. 4995–4996.

[27] S. I. Ktena, S. Parisot, E. Ferrante, M. Rajchl, M. Lee, B. Glocker, and D. Rueckert, "Metric learning with spectral graph convolutions on brain connectivity networks," *NeuroImage*, vol. 169, pp. 431–442, 2018. [Online]. Available: https://www.sciencedirect.com/science/article/pii/S1053811917310765

[28] M. Zhang, Y. Liang, and H. Ma, "Context-aware affective graph reasoning for emotion recognition," in *2019 IEEE International Conference on Multimedia and Expo (ICME)*, 2019, pp. 151–156.

[29] Q. Gao, H. Zeng, G. Li, and T. Tong, "Graph reasoning-based emotion recognition network," *IEEE Access*, vol. PP, pp. 1–1, 01 2021.

[30] H.-I. Suk, C.-Y. Wee, S.-W. Lee, and D. Shen, "State-space model with deep learning for functional dynamics estimation in resting-state fmri," *NeuroImage*, vol. 129, pp. 292–307, 2016. [Online]. Available: https://www.sciencedirect.com/science/article/pii/S1053811916000100

[31] D. Wen, Z. Wei, Y. Zhou, G. Li, X. Zhang, and W. Han, “Deep learning methods to process fmri data and their application in the diagnosis of cognitive impairment: a brief overview and our opinion,” *Frontiers in neuroinformatics*, vol. 12, p. 23, 2018.

[32] A. Riaz, M. Asad, E. Alonso, and G. Slabaugh, “Deepfmri: End-to-end deep learning for functional connectivity and classification of adhd using fmri,” *Journal of neuroscience methods*, vol. 335, p. 108506, 2020.

[33] B. Biswal, F. Z. Yetkin, V. M. Haughton, and J. S. Hyde, “Functional connectivity in the motor cortex of resting human brain using echo-planar MRI,” *Magn. Reson. Med.*, vol. 34, no. 4, pp. 537–541, Oct. 1995.

[34] J. S. Damoiseaux, S. A. R. B. Rombouts, F. Barkhof, P. Scheltens, C. J. Stam, S. M. Smith, and C. F. Beckmann, “Consistent resting-state networks across healthy subjects,” *Proc. Natl. Acad. Sci. U. S. A.*, vol. 103, no. 37, pp. 13 848–13 853, Sep. 2006.

[35] K. A. Smitha, K. Akhil Raja, K. M. Arun, P. G. Rajesh, B. Thomas, T. R. Kapilamoorthy, and C. Kesavadas, “Resting state fMRI: A review on methods in resting state connectivity analysis and resting state networks,” *Neuroradiol. J.*, vol. 30, no. 4, pp. 305–317, Aug. 2017.

[36] J. Yang, S. Gohel, and B. Vachha, “Current methods and new directions in resting state fMRI,” *Clin. Imaging*, vol. 65, pp. 47–53, Sep. 2020.

[37] D. S. Bassett and E. T. Bullmore, “Human brain networks in health and disease,” *Current opinion in neurology*, vol. 22, no. 4, p. 340—347, August 2009.

[38] J. Zhang, J. Wang, Q. Wu, W. Kuang, X. Huang, Y. He, and Q. Gong, “Disrupted brain connectivity networks in drug-naive, first-episode major depressive disorder,” *Biological Psychiatry*, vol. 70, no. 4, pp. 334–342, 2011.

[39] W. Huang, L. Goldsberry, N. F. Wymbs, S. T. Grafton, D. S. Bassett, and A. Ribeiro, “Graph frequency analysis of brain signals,” *IEEE Journal of Selected Topics in Signal Processing*, vol. 10, no. 7, pp. 1189–1203, 2016.

[40] W. Huang, T. Bolton, J. Medaglia, D. Bassett, A. Ribeiro, and D. Van De Ville, “A graph signal processing perspective on functional brain imaging,” *Proceedings of the IEEE*, vol. PP, pp. 1–18, 03 2018.

[41] S. Gao, X. Xia, D. Scheinost, and G. Mishne, “Smooth graph learning for functional connectivity estimation,” *NeuroImage*, vol. 239, p. 118289, 2021.

[42] H. Li, T. D. Satterthwaite, and Y. Fan, “Large-scale sparse functional networks from resting state fMRI,” *NeuroImage*, vol. 156, pp. 1–13, 2017.

[43] S. Batreddy, A. Siripuram, and J. Zhang, "Robust graph learning for classification," *Signal Processing*, vol. 211, p. 109120, 2023.

[44] H. Eavani, T. D. Satterthwaite, R. Filipovych, R. E. Gur, R. C. Gur, and C. Davatzikos, "Identifying sparse connectivity patterns in the brain using resting-state fMRI," *NeuroImage*, vol. 105, pp. 286–299, 2015.

[45] M. W. Cole, D. S. Bassett, J. D. Power, T. S. Braver, and S. E. Petersen, "Intrinsic and task-evoked network architectures of the human brain," *Neuron*, vol. 83, no. 1, pp. 238–251, 2014.

[46] Statistical Parametric Mapping (SPM), "SPM12," *Wellcome Trust Centre for Neuroimaging*, 2014. [Online]. Available: https://www.fil.ion.ucl.ac.uk/spm/software/spm12

[47] B. Holla, P. A. Taylor, D. R. Glen, J. A. Lee, N. Vaidya, U. M. Mehta, G. Venkatasubramanian, P. K. Pal, J. Saini, N. P. Rao *et al.*, "A series of five population-specific indian brain templates and atlases spanning ages 6–60 years," *Human Brain Mapping*, vol. 41, no. 18, pp. 5164–5175, 2020.

[48] R. A. Poldrack, J. A. Mumford, and T. E. Nichols, *Handbook of Functional MRI Data Analysis*. Cambridge University Press, 2011.

[49] K. R. Van Dijk, M. R. Sabuncu, and R. L. Buckner, "The influence of head motion on intrinsic functional connectivity mri," *NeuroImage*, vol. 59, no. 1, pp. 431–438, 2012, neuroergonomics: The human brain in action and at work. [Online]. Available: https://www.sciencedirect.com/science/article/pii/S1053811911008214

[50] J. D. Power, K. A. Barnes, A. Z. Snyder, B. L. Schlaggar, and S. E. Petersen, "Spurious but systematic correlations in functional connectivity mri networks arise from subject motion," *NeuroImage*, vol. 59, no. 3, pp. 2142–2154, 2012. [Online]. Available: https://www.sciencedirect.com/science/article/pii/S1053811911011815

[51] X. Shen, F. Tokoglu, X. Papademetris, and R. Constable, "Groupwise whole-brain parcellation from resting-state fmri data for network node identification," *NeuroImage*, vol. 82, pp. 403–415, 2013. [Online]. Available: https://www.sciencedirect.com/science/article/pii/S1053811913005818

[52] G. H. Glover, "Deconvolution of impulse response in event-related bold fmri1," *Neuroimage*, vol. 9, no. 4, pp. 416–429, 1999.

[53] S. M. Smith, K. L. Miller, G. Salimi-Khorshidi, M. Webster, C. F. Beckmann, T. E. Nichols, J. D. Ramsey, and M. W. Woolrich, "Network modelling methods for fmri," *Neuroimage*, vol. 54, no. 2, pp. 875–891, 2011.

[54] L. Griffanti, M. Rolinski, K. Szewczyk-Krolikowski, R. A. Menke, N. Filippini, G. Zamboni, M. Jenkinson, M. T. Hu, and C. E. Mackay, "Challenges in the reproducibility of clinical studies

with resting state fmri: An example in early parkinson's disease," *Neuroimage*, vol. 124, pp. 704–713, 2016.

[55] X. Dong, D. Thanou, P. Frossard, and P. Vandergheynst, "Learning laplacian matrix in smooth graph signal representations," *IEEE Transactions on Signal Processing*, vol. 64, no. 23, pp. 6160–6173, 2016.

[56] J. Friedman, T. Hastie, and R. Tibshirani, "Sparse inverse covariance estimation with the graphical lasso," *Biostatistics*, vol. 9, no. 3, pp. 432–441, Jul. 2008.

[57] R. Tibshirani, "Regression shrinkage and selection via the lasso," *Journal of the royal statistical society series b-methodological*, vol. 58, pp. 267–288, 1996.

[58] S. GRS, "Brain-connectivity-fMRI," https://github.com/Sasanka-GRS/Brain-connectivity-fMRI, Apr. 2024.

[59] F. Murtagh and P. Legendre, "Ward's hierarchical agglomerative clustering method: which algorithms implement ward's criterion?" *Journal of classification*, vol. 31, pp. 274–295, 2014.

[60] C. Lamm, J. Decety, and T. Singer, "Meta-analytic evidence for common and distinct neural networks associated with directly experienced pain and empathy for pain," *NeuroImage*, vol. 54, no. 3, pp. 2492–2502, 2011. [Online]. Available: https://www.sciencedirect.com/science/article/pii/S1053811910013066

[61] Y. Zhu, H. Gao, L. Tong, Z. Li, L. Wang, C. Zhang, Q. Yang, and B. Yan, "Emotion regulation of hippocampus using real-time fMRI neurofeedback in healthy human," *Front. Hum. Neurosci.*, vol. 13, p. 242, Jul. 2019.

[62] K. Sergerie, C. Chochol, and J. L. Armony, "The role of the amygdala in emotional processing: a quantitative meta-analysis of functional neuroimaging studies," *Neurosci. Biobehav. Rev.*, vol. 32, no. 4, pp. 811–830, Jan. 2008.

[63] A. Caria, R. Sitaram, R. Veit, C. Begliomini, and N. Birbaumer, "Volitional control of anterior insula activity modulates the response to aversive stimuli. a real-time functional magnetic resonance imaging study," *Biol. Psychiatry*, vol. 68, no. 5, pp. 425–432, Sep. 2010.

[64] S. GRS, "Brain-connectivity-fMRI-resting-state," https://github.com/Sasanka-GRS/Brain-connectivity-fMRI-resting-state, Mar. 2024.

[65] R. E. Gabry, "This Time — by Ramy El Gabry," https://www.youtube.com/watch?v=l9bbUJRv2JI, Aug. 2011.

[66] P. M. Castillo, "Most the movie (subtitulos Español) Complete," https://www.youtube.com/watch?v=E9pNv4B9sxc, Aug. 2016.